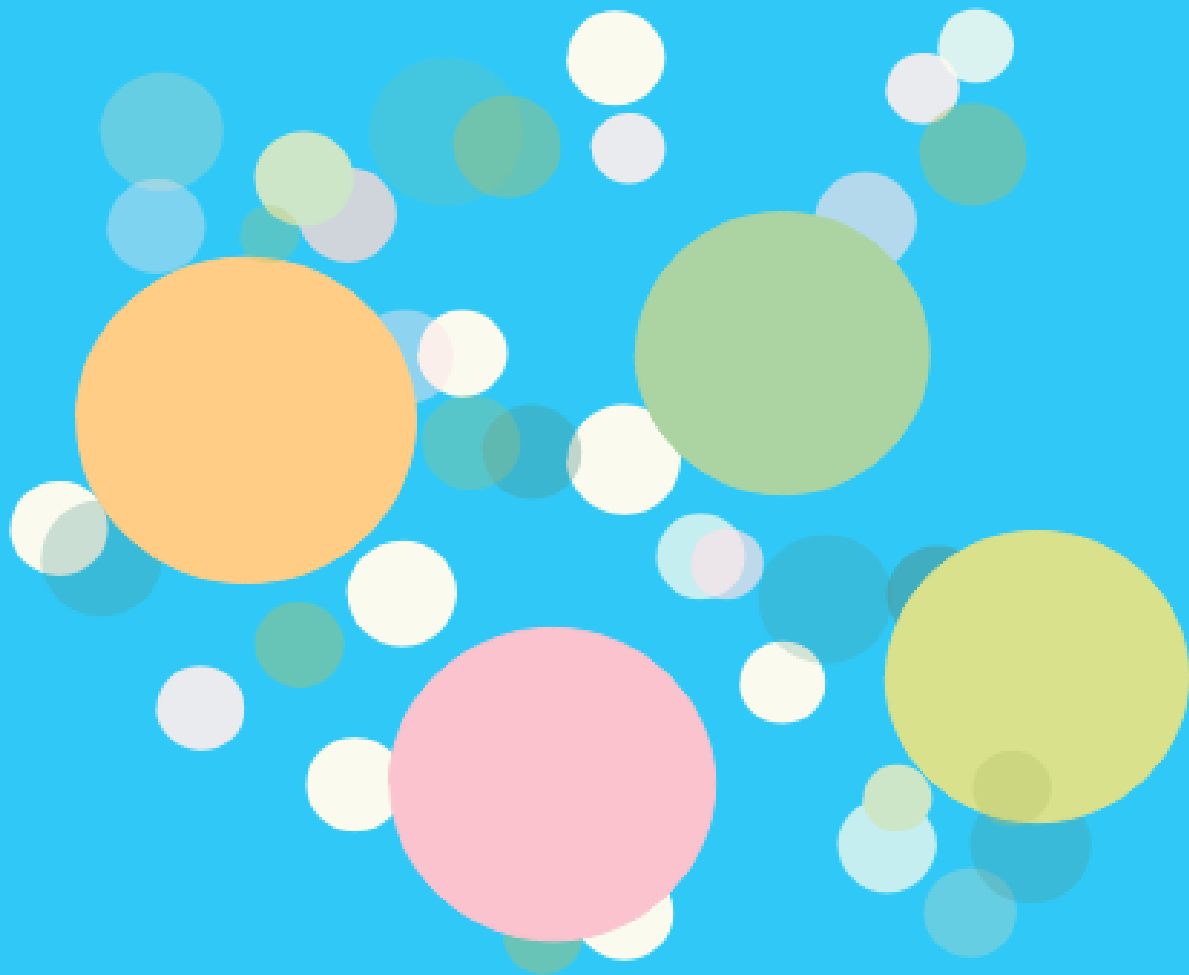# Cannabinoid encapsulating nanoparticles for atherosclerosis therapy

An in vitro study

Amel Nouar (4246500)

TUDelft

Delft
University of
Technology

Challenge the future

Cannabinoid encapsulating nanoparticles for atherosclerosis therapy

An in vitro study

by

Amel Nouar (4246500)

in partial fulfillment of the requirements for the degree of

Master of Science
in Biomedical Engineering

at the Delft University of Technology,
to be defended publicly on Thursday August 24, 2017 at 08:30 AM.

Supervisors:	Dr. ir. I. Apachitei	TU Delft
	Dr. A. Zadpoor	TU Delft
	T. J. Beldman,	AMC Amsterdam
Thesis committee:	Dr. A. Zadpoor	TU Delft
	Dr. ir. I. Apachitei	TU Delft
	T. J. Beldman,	AMC Amsterdam

TUDelft
Delft
University of
Technology

Abstract

Atherosclerosis, the chronic inflammation of the arterial wall, is one of the leading causes of death in the western societies. Which is characterized by the accumulation of inflammatory macrophages and necrotic regions in the intima. Rupture of the plaque can lead to thrombosis, a blood clot in the blood vessel, blocking the natural flow of the blood. If left untreated the entire lumen can be blocked and the results can be fatal. Progression in atherosclerosis is mainly driven by the build up of macrophages. An important phenotype on these cells are cannabinoid receptors, important in the control of inflammatory pathways. By presenting inflammatory relieving cannabinoids to these receptors, the macrophages could become less inflammatory. A localized delivery would give the additional benefit of reducing systematic side effects. High density lipoprotein based nanoparticles have shown to be great carriers for drug molecules. Additionally, high density lipoproteins are able to relieve AS up to a certain extend. In this research we analyzed physical and physio-chemical properties of different nanoparticle formulations. Specifically, the size, morphology and ζ-potential. Next we investigated the cannabinoid receptor expression on different types of macrophages, which verified that macrophages in atherosclerotic conditions have an abundance of our target receptor. Finally we performed a small *in vitro* study showing both empty and cannabinoid loaded nanoparticles relieved pro-inflammatory signals.

Abbreviations

ABCA-1	ATP-binding cassette transporter 1
Acetyl-LDL	Acetylated low density lipoprotein
AS	Atherosclerosis
ApoA1	Apolipoprotein A1
BCA	Bicinchoninic acid
CBD	Cannabidiol
DAPI	4,6-Diamidino-2-Phenylindole
DLS	Dynamic light scattering
DMPC	1,2-dimyristoyl-sn-glycero-3-phosphocholine
ELISA	Enzyme-Linked Immuno Sorbent Assay
FBS	Fetal bovine serum
HDL	High density lipoprotein
ICAM-1	Intracellular adhesion molecule
IFNγ	Interferon gamma
IL-x*	Interleukine-x*
LCM	L929 conditioned medium
LC-MS	Liquid chromatography–mass spectrometry
LDL	Low density lipoprotein
LPS	Lipopolysaccharide
M-CSF	Macrophage colony-stimulating factor
MCP-1	Monocyte chemotactic protein 1
MHPC	1-myristoyl-2-hydroxy-sn-glycero-3-phospho-(1′-rac-glycerol)
MTT	3-(4,5-Dimethylthiazol-2-yl)-2,5-diphenyltetrazoliumbromidefor
NO	Nitric Oxide
NPs	Nanoparticles
Ox-LDL	Oxidized low density lipoprotein
PBS	Phosphate-buffered saline
PHPC	1-palmitoyl-2-hexadecyl-sn-glycero-3-phosphocholine
PLA	Poly(lactic-acid)
PLGA	Poly(Lactide-co-Glycolide)
POPC	1-palmitoyl-2-oleoyl-sn-glycero-3-phosphocholine
TEM	Transmission electron microscopy
TMB	TMB-ELISA Substrate Solution
TNFα	Tumornecrosefactorα
VCAM-1	Vascular cell adhesion molecule 1

* x being a natural number (e.g. 1, 6 or 12).

Contents

1

Introduction

1.1. Atherosclerosis development

Cardiovascular diseases have become one of the primary causes of mortality in western societies over the last few decades [1]. Around 68% of these cases are caused by atherosclerosis (AS), characterized by the chronic inflammation in the blood vessel walls [2]. The predominant trigger for AS is the diffusion of low density lipoprotein (LDL) into the tunica *intima* (innermost layer of the arterial wall) [3][4][5]. A series of events result into the expansion of *intima* and subsequently the narrowing of the lumen, disrupting the natural flow of the blood. In later stages the entire artery becomes blocked and tissue and cell death occurs posterior to the blockage. Strokes and infarcts are clear examples of entire organs being drained from blood supply. Traditionally six different phases are distinguished although most developments overlap in time [5]. In Figure 1.1 the different stages in AS are further illustrated.

1.1.1. Lipid deposition

A high concentration of LDL in the lumen, usually caused by poor lifestyle or genetic disorder, will diffuse, around the endothelial cells, into the *intima* by Fick's law. The main function of the endothelial cells is to manage permeability of cells and molecules (e.g. leukocytes and LDL) and to act as a barrier. Another important function is to create a smooth surface for minimal friction between the blood and the wall, a function which is greatly disturbed in AS later stages. The LDL is able to undergo electrostatic interaction with the proteoglycans, oxidizing the LDL (Ox-LDL). Oxidization of LDL is relatively easy compared to high density lipoprotein (HDL) due to the rich fatty acid content and poor cholesterol ester content in LDL [6]. Further interactions with extracellular matrix proteins and cells stress the endothelium [7].

1.1.2. Endothelium defences

The resulted stress on the endothelium increases its permeability, which has been correlated to AS development [8]. A switch in physiological and functional phenotype is initiated and will be remaining for the entire progression. A discrete distribution of anionic sites in their cell membrane, opposed to the common homogeneous arrangement, can be observed. A study suggests that this rearrangement further increases the permeability for LDL [9]. Another essential alternation in endothelial cell physiology is the formation of new cell molecules such as ICAM-1 (intercellular adhesion molecule), E-selecting and P-selectin (both employ in the recruitment of monocytes), as well as VCAM-1 (vascular cell adhesion molecule) just to name a few [3]. Other monocyte attractors for monocytes are also synthesized, Monocyte chemotactic protein 1 (MCP-1) and Interleukin-8 (IL-8) for instance (Figure 1.1). Oftentimes these molecules are overexpressed in AS plaque. Endothelial cells also express specific cytokines targeting smooth muscle cells in the middle layer of the arterial wall (tunica *media*). In healthy conditions the media and its content allows for vasoconstriction and vasodilation of the wall, regulating pressure and temperature [7]. However in atherosclerotic conditions the smooth muscle cells are triggered to switch their phenotype to a synthetic phase [10] [11].
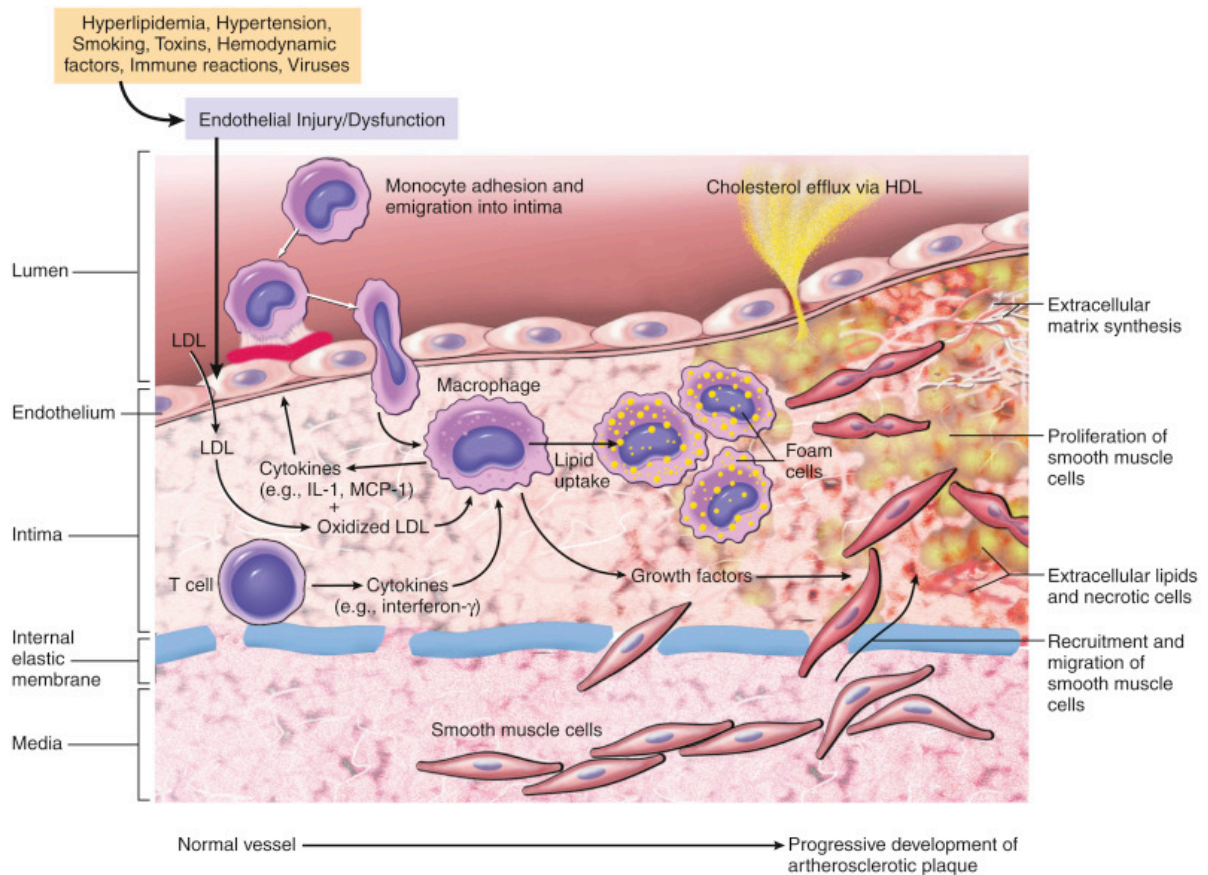
Figure 1.1: **The different stages with their contributing cells and signals in AS development [5].** Several key factors can lead to the development of AS (yellow box) (e.g. high fat diet or stress). This will lead to a disruption of the endothelium, allowing LDL to enter the *intima*. These become oxidized which will ultimately attract white blood cells to clean up. Macrophages embed the Ox-LDL and become foam cells, unable to escape the lesion. The foam cells will die and release their content into the extracellular matrix forming calcified nectrotic cores. Simultaneously smooth muscle cells are recruited from the *media* which will secrete atherogenetic cytokines. Ruptures in the plaque will release the inflammatory content into the lumen progressing the disease further by initiating thrombosis. On the other hand cholesterol and LDL can be modified and extracted from the cells and *intima* in a HDL complex, relieving stress from the endothelium.

1.1.3. Leukocyte recruitment

As mentioned previously MCP-1 and IL-8 are expressed to recruit leukocytes, specifically dendritic cells, T lymphocytes and plasma monocytes. It has been shown that dendritic cells main function is to present antigens to T lymphocytes, since they are often observed to be in direct contact or at short distances in the AS plaque [11]. Specifically the dendritic cell type $CD86^+CD11C^+$ is often detected in the *intima* layer and most likely recruited by VCAM-1 [3]. Macrophages are one of the differentiated forms of monocytes and play an important role in regulating inflammation and in removal of dead cells. Two distinct monocyte subsets (CD14$^+$CD16$^+$ and CD14$^+$CD16^{low}) are to be recruited by the endothelial cells and triggered to enter the *intima*.

Platelets also play an important role in the AS progression. The modified endothelial cells emit specific von Willebrand factors which aid in the regulation of hemostasis [5] [12]. In turn the platelets secrete pro-inflammatory attractors such as Matrix metalloproteinase, P-selectin and CD40 ligands. Monocytes are promoted to bind to VCAM-1 hence increasing their adhesiveness. Macrophage scavenger receptors are present on the monocyte surface and are able to recognize Ox-LDL and are believed to play a key role in macrophage differentiation. Macrophages in turn exhibit increased levels of Macrophage scavenger receptors on the surface and are able to encapsulate Ox-LDL [13]. The high Ox-LDL uptake causes the macrophages to develop a foamy phenotype, called foam cells, which upon themselves are not dangerous but in high numbers can induce necrotic areas.

1.1.4. Lipid lesion formation

Damaged vessels stimulate platelets to release chemical agents attracting other platelets and leukocytes to the scene, creating a positive feedback system. In parallel the macrophages keep digesting the Ox-LDL, developing the foamy phenotype. Foam cells are highly fat loaded macrophages that emit various factors including, reactive oxygen species that induce chronic inflammation, different from regular macrophages. Both the vessel damage and release of reactive oxygen species stimulate the smooth muscle cells to undergo a series of changes.

Healthy smooth muscle cells show to be spindle shaped with many contractile filaments. They also show a relatively low proliferation and migration capacity. However during AS development they seem to polarize toward a more *synthetic* phenotype (Figure 1.2). Proliferation and migration rates increase and, morphologically speaking, form a more rectangular shape [10] [11]. The smooth muscle cells migrate into the *intima* and start producing extracellular matrix proteins including, collagen, laminin, elastin and glycoproteins (Figure 1.1). These proteins play key roles in the support of lipid lesions, in cell migration and proliferation. Together with the macrophages atherogenic cytokines are released such as Tumornecrosefactorα (TNFα), IL-1β, IL-6, IL-12 and Nitric Oxide (NO) [10].

- Proliferating (cell division occuring)
- Migrating (able to invade)
- Noncontractile
- Secretory/ Synthetic (synthesizing extra-cellular matrix)
- Rhomboid shape

- Nonproliferating
- Nonmigrating
- Contractile (smc contractile protein organized in fibers)
- Focal adhesions and integrin receptors connect contractile fibers to ECM
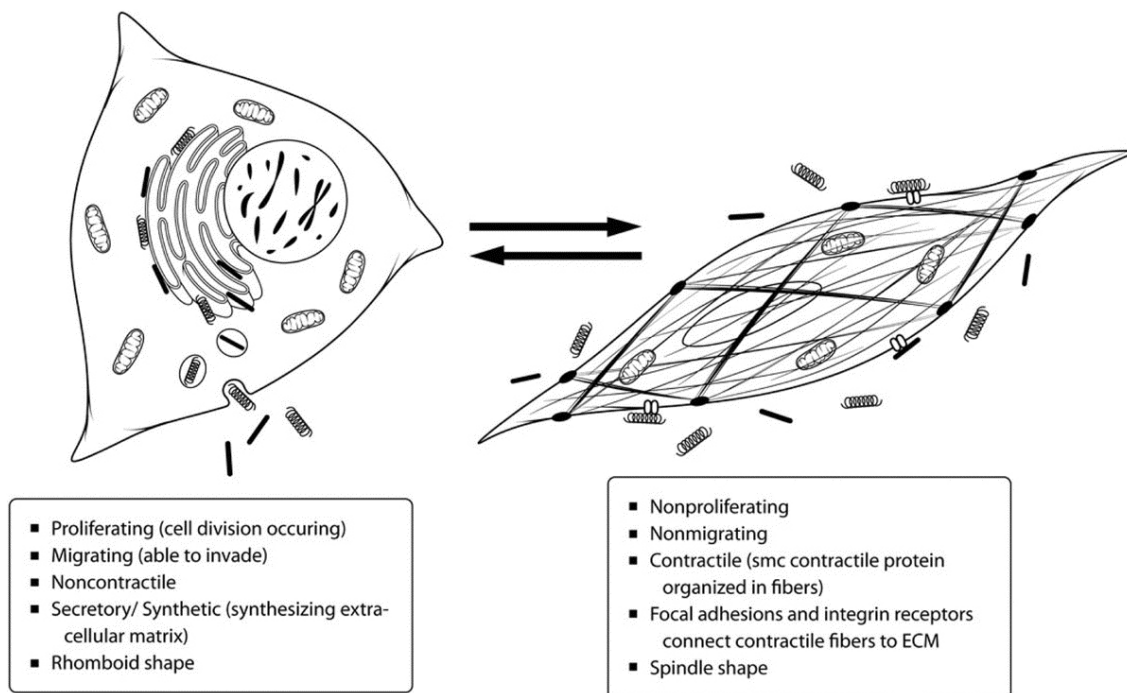- Spindle shape

Figure 1.2: **The two different types of smooth muscle cells.** The synthetic smooth muscle cell phenotype (left) and the general phenotype (right) with the key characteristics [11]. The synthetic smooth muscle cell has an endoplasmic reticulum that is important for protein synthesis. The general smooth muscle cell has more contractile fibers and less synthesized proteins.

The inflammatory defense mechanisms is considered to be the immune systems method of relieving the contact of the inflammatory-induced region and the blood. The cells involved try to gather the lipid droplets, creating a fibrous cap, but consequently forming lipid-lesions in the inflammatory-induced region. A simplistic method of studying the macrophages is by using the dual polarity concept (Figure 1.3). In this model a macrophage can be of M1 or M2 type macrophage. M1 polarized macrophages are considered the pro-inflammatory macrophages which are the main drive for recruitment and inflammation. On the contrary M2 polarized macrophages exhibit anti-inflammatory properties [14].

These cells exhibit a large amount of cannabinoid receptors on their surfaces, which play an important role in regulating inflammation. The two main receptors are the CB_1 and CB_2 type receptors [15]. During chronic inflammation specific cannabinoid ligands can interact with these receptors and promote either a pro-inflammatory or anti-inflammatory pathways. Stimulation can be achieved by agnostic ligands whereas antagnostic ligands can be used to block the posterior pathway [16]. Because CB_2 is the main cannabinoid receptor type in immune cells it is wise to target this pathway. A further detailed description is presented in section 1.3 (Novel treatment).
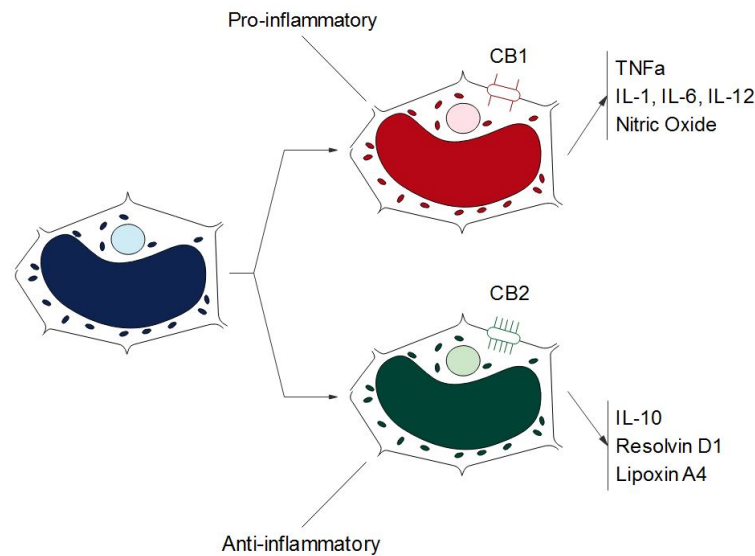
Figure 1.3: **Schematic illustration representing the dual polarity theory of macrophages, based on the description of Nakagawa et al. [14]**. A neutral macrophage (blue) is able to polarize into a pro-inflammatory M1 type (red) or an anti-inflammatory M2 type (green). They excrete different cytokines with pro- or anti-inflammatory properties. On type M1 CB_1 receptors stimulate pro-inflammatory signaling while on M2 CB_2 receptors stimulate anti-inflammatory pathways. Both receptors are present on both types. However $CB1$ and CB_2 are most predominantly present in M1 and M2 respectively.

1.1.5. Necrotic core and calcification

There are three fates of a macrophage in AS plaque. Apoptosis, cell death, is one of these fates. Apoptotic macrophages, foam cells and smooth muscle cells release their content in the extracellular matrix and lesion. Unesterified Ox-LDL regions, TNFα and -β in high amounts are factors that induce endoplasmic reticulum stress [17]. This is achieved by the improper protein folding after translation. Protein misfolding triggers an unfolded protein response aiming to protect the cell. In the short run this is achieved by degrading existing misfolded proteins, stopping protein translation and stimulating chaperone production. If prolonged endoplasmic reticulum stress is present and the unfolded protein short-term response goals are not reached, the systems will initiate apoptosis. Due to environmental restrictions the dead cells are not removed by the body and necrotic cores are formed rich in calcium content. The cell content will diffuse into the extracellular matrix forming cholesterol crystals. Whereas the initial lipid lesions within a fibrous capsule is considered to be stable and not dangerous, the calcified necrotic cores and cholesterol crystals weakening the fibrous capsule, forming unstable and dangerous regions. The secretion of cytokines aid in the digestion of the extracellular matrix further weakening the tissue.

1.1.6. Plaque rupture and thrombosis

Another effect of the endoplasmic reticulum stress, induced by the oxidized lipids, is the increasing signaling of inflammatory cytokines and recruiting new cells. Additionally the endothelial cells parting the lumen and the lipid core will thinner, easing cell migration. Matrix metalloproteinases are also secreted, which are involved in the digestion of different extracellular matrix proteins such as collagen. The migration of smooth muscle cells has also led to a decrease in smooth muscle cells in the *media* since proliferation is limited in this region. Resulting in more difficult control of blood pressure and temperature regulation. *Synthetic* smooth muscle cells in the plaque core further secrete calcium, hardening the structure. The increasing volume of the plaque lesion will directly lead to the narrowing of the lumen disrupting the natural blood flow [5]. The endothelial surfaces roughens and erodes creating more friction on the interface. The thinned fibrous cap together with the increased pressure on the endothelial cell barrier and endothelial cell erosion form a treat for plaque rupture leading to thrombosis.

Rupture of the lesion leads to the exposure of its content to the circulating blood in the lumen. When the damaged tissue comes in contact with the blood it starts to secrete thromboplastin substances. A chain reaction, which requires calcium, is started that eventually will make the platelets

release prothrombin activators, initiating blood clotting. The calcium helps convert the prothrombin into thrombin, catalyzing the formation of long strong chains of fibrin. The fibrin treads form a mesh onto the damaged region holding platelets and erythrocytes in place [18]. If the rupture and clotting are not lethal the thrombus will start to shrink, heal and remodel (Figure 1.4).
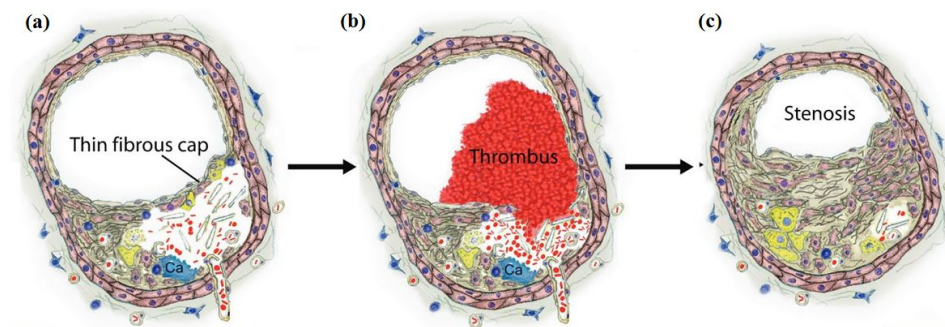

Figure 1.4: **Thrombosis and stenosis development in the arterial walls.** The weakening of the fibrous cap and final rupturing (a) the thromboplastin substances stimulate blood clotting forming a thrombus (b). If after healing the rupture is non-lethal a stenosis forms (c) [4].

During remodeling the lumen is often narrower than before the rupture forming a stenosis. Additional ruptures are not exclude and often the lumen keeps narrowing until blood is unable to pass through. The blockage of oxygen delivery and carbon-dioxide removal of the cells posterior to the blood clot leads to cell death which can be lethal.

1.2. Atherosclerosis current treatments

Treatments are usually performed after severe narrowing of the arteries since the early signs are undetectable. The main goals of any AS treatment are to lower thrombosis risks, decelerate plaque accumulation and relieve symptoms (e.g. pain). Dependent on the severity of the inflammation three different treatments can be applied. The first method relies on medication, the second on an implant and the last method is a bypass surgical procedure.

1.2.1. Medication

Medication is usually given when the risks of thrombosis development are relatively low. In this case the main goal is to decelerate the AS progression and postpone complications. One common strategy used is lowering LDL levels in the blood system, which can be achieved by using Statin medication [19]. This is achieved by increasing the LDL uptake by the liver and decreasing LDL synthesis. Two independent studies showed the benefits of this approach [19][20]. On the other hand there have been some controversial studies conducted addressing the safety issues with Statin on a systematic level. One review specifically argues that the use of Statin induces heart failures by disrupting selenoprotein synthesis [21]. Statin could be toxic for mitochondria and damage cells. Despite the review citing different studies which express similar results, Statin is still prescribed for AS treatment. Reducing blood clotting is another tactic used to decelerate thrombosis development, which can be achieved by medication such as Aspirin. The formation of a stenosis is mainly the result of platelets accumulation on the rupture site, Aspirin could decelerate the process. However blood thinning could come with a serious disadvantage in a patient's personal life. Another commonly used oral treatment is used to lower the general blood pressure on a systematic level. The idea behind this approach is the effect the blood pressure on the endothelium. The cells and tissue will further be stretched and weakened. Blood thinning using antiplatelet is a final medicine based approach to combat AS development. Aspirin is a commonly purchased example, blood thinning reduces the formation of blood clots and postpones thrombosis.

1.2.2. Stenting and bypass surgery

When medicines will not be adequate a medical procedure will be performed, usually this applies for high thrombosis or stenosis risks. With an angioplasty a catheter is positioned in the narrowed region. With a secondary catheter a balloon is inflated in the narrowed artery, expanding the lumen. Simultaneously

a stent is widened with the balloon which will stay in place while the catheters and balloon are removed. The stent keeps the artery open and allows for the blood to flow again (Figure 1.5) [22]. The stents used have a lot of variety such as the geometrical structure, and the materials used. Most stents on the market are build up from a metallic platform, such as cobalt chromium and stainless steel [23]. In the last years new stents with biodegradable properties were developed, however these are not commercialized yet. Some have specific coatings that should improve the therapeutic outcome, some compounds are used to affect the cellular response of the foreign body while others try to attack the plaque itself. However most of these coatings are still in the early clinical or animal studies.

With a bypass surgery a part of the patients veins (usually from the lower limbs) is removed and surgically added around the narrowed artery. As the name suggests the blood is redirected along the new vein and around the atherosclerotic region. This is usually only done for coronary arteries and is more difficult for aortic problems [24].
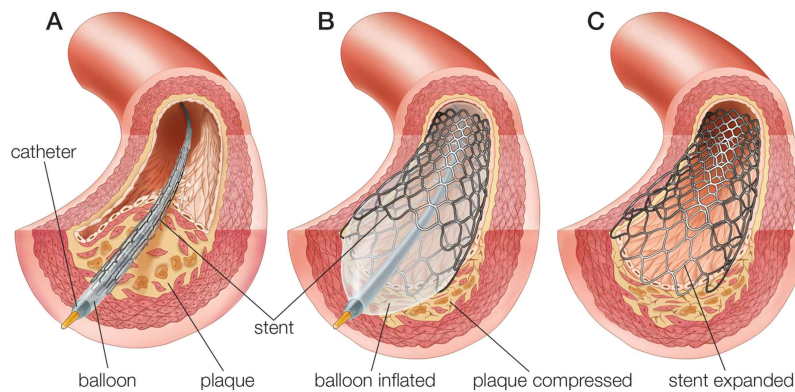

Figure 1.5: **Illustration of a catheter and stent positioning (angioplasty)**. The folded stent is inserted in the vessel close to the region of interest (a). A second catheter is also inserted and a balloon is inflated, widening the stent and compressing the plaque (b). The catheters are then removed and the stent is said in place (c) [25].

1.3. Novel approach

There is a limited extend to which the above mentioned therapies can aid. Medication is only able to decelerate the process of AS and both stenting and bypass surgery only provide a solution to a single AS site. It does not treat or regress AS on different sites. The main issues pushing AS development are entrapment of both (Ox)-LDL and macrophages in the *intima* (1), the continuous recruitment of new cells (2), chronic pro-inflammatory signalling (3) and the increasing blockage of the lumen (4). These factors keep the progression of AS going and limit the recovery of the tissue. As mentioned in the sections 1.1.4 and 1.1.5, the endocannabinoid system plays an important role in regulating inflammation. Upon further research it becomes clear that the endocannabinoid system can, potentially, be used in a novel therapy in AS.

1.3.1. Role of cannabinoids in atherosclerosis

Research has shown that the macrophage uptake of Ox-LDL activates the endocannabinoid system, specifically cannabinoid receptor protein translation [26]. These receptors can be found on the cell membrane and can induce inflammatory pathways by cannabinoid ligands [27]. Cannabinoid compounds, such as Δ-9-tetrahydro-cannabinol, have been used for centuries in medicine and recreation [16]. In the last decades many cannabinoid ligands have been discovered and synthesized with different affinity for CB_1 and CB_2. Most cannabinoid ligands are lipid based and have hydrophobic properties [16]. Some have agnostic affinity, meaning a stimulation of the posterior pathway, while others have an antagonistic affinity, blocking the receptor and subsequently the posterior pathway [28] [29].

AM251, an effective CB_1 antagonist ligand, increased ATP-binding cassette transporter ABCA1 (ABCA-1) protein expression under AS mimicked conditions (Ox-LDL incubated macrophages) [26]. ABCA-1 is a membrane protein regulating cholesterol efflux (Figure 1.1). Together with ATP-binding cassette sub-family G member 1, another cholesterol efflux regulator, it is responsible for 70% of

cholesterol efflux and HDL formation of a cell [30]. One model suggests that the interaction of ApoA1, present on HDLs, with cell surface receptors induces the transportation of cholesterol to the interaction site [31]. ABCA-1 promotes cholesterol and ApoA1 to form HDL complexes, which will thus release the cholesterol from the cell. The removal of the cholesterol is the first step in the reverse cholesterol transport mechanism. Ultimately the modified cholesterol, embedded in the HDLs, can be transported to the liver before leaving the body via the bile [32] [33].

Taking a step back three ultimate fates can be categorized for a macrophage has in the lesion (Figure 1.6). The first one is related to the inflammation and is characterized by pro-inflammatory cytokine production and cell recruitment molecule secretion. Secondly, and often a result from the first category, is cell death contributing to necrotic core formation and calcification. Finally the category of cells that is still able to escape from the lesion. In the final category limited Ox-LDL, cholesterol crystals and free droplets are present, allowing it to escape the *intima*. This can be achieved by a relative high efflux of cholesterol in the shape of HDL. ABCA-1 is able to remove excess cholesterol which has shown to be important in inflammatory responses [30]. By promoting the ABCA-1 cell membrane protein, using the cannabinoid pathway and the HDL structures, the macrophage is able to modulate the Ox-LDL and decrease the chance of becoming a pro-inflammatory macrophage or of dying [15].
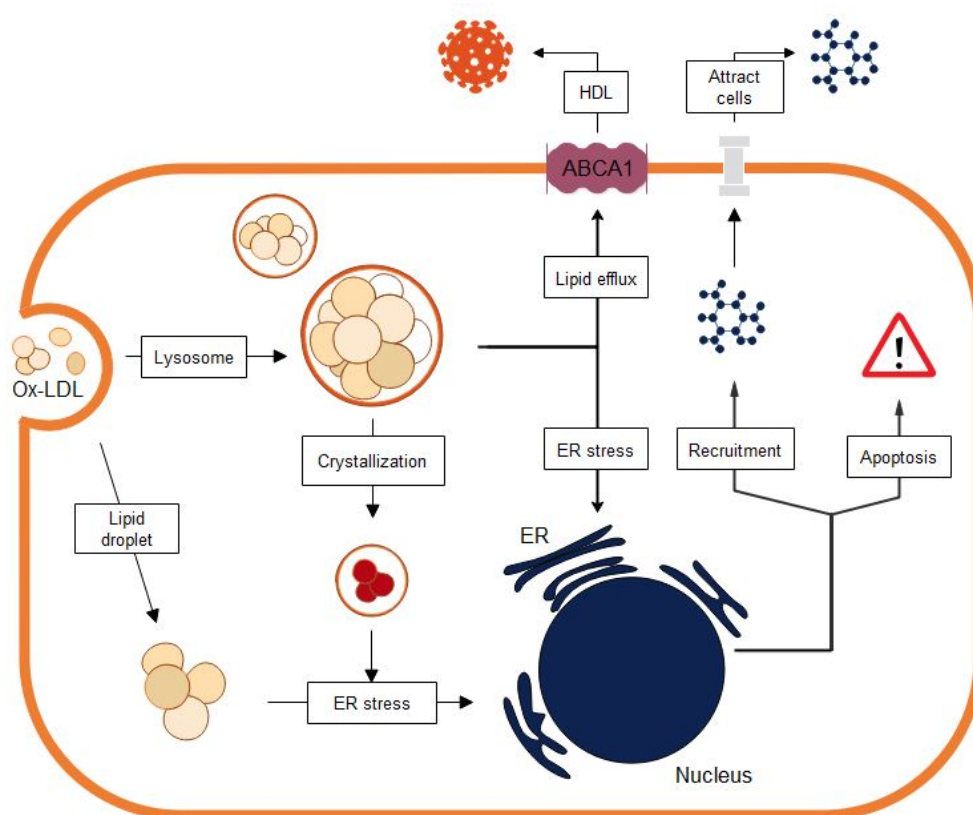

Figure 1.6: **Schematic representation of the cellular paths in AS, specifically macrophages**. (a) Ox-LDL is able to fuse into the cell (orange) either in the shape of lysosomes or as loose lipid droplets. These will circulate in the cell and are able to crystallize (depicted in red). The different shapes the Ox-LDL in the cell can induce stress on the ER (blue). It low doses this induces protein translation related to inflammation and cell recruitment. In higher doses an unfold protein response is triggered, which in the long run induces apoptosis. Cholesterol can also be modulated by the ABCA1 cell membrane protein (purple). Together with ApoA1 and phospholipids high density lipoproteins (HDL) can be synthesized [14].

1.3.2. Localized treatment using high density lipoprotein nanoparticles
HDLs are primarily made up of a phospholipid and an ApoA1 embedded surface and a triglyceride and cholesteryl ester fatty core [34]. Besides the interaction with the cell surface receptors ApoA1 improves the stability of the HDL particles [35]. The removal of lipids and cholesterol from cells and tissues plays an important role in AS. However, they cannot fully regress AS single-handedly [33]. In the last decades however, reconstituted HDL particles were designed to carry hydrophobic drug molecules to cells and

tissues [36]. Various studies have already presented promising results in mouse studies, showing the specificity of the delivery [34] [37] [38] [39].

Promoting the HDL synthesis by modulating the cholesterol in the cells would be a way to stop cell apoptosis, and therefore necrotic core formation, and stop pro-inflammatory signalling. This can be achieved using the endocannabinoid system. Specific cannabinoid ligands blocking CB_1 and promoting CB_2 induced pathways on both M1 and M2 type macrophages can be used.

Ideally delivering these ligands locally would boost the drug efficiency and relieve more systematic side effects. These can be achieved by a delivery system with a distinct target. Nanoparticles (NPs) have been used to deliver hyaluronan, important in atherogenesis regulation, to AS lesions. It induced anti-inflammatory signalling and repress pro-inflammatory signalling [40]. NPs have the potential of delivering specific factors to targeted regions in the body. They usually remain in the range of 10 to 100 nm and are build up of an outer shell and inner core. Their size limits extraction from the blood hence increasing the circulation time. At the AS site the permeability is increased which allows for an easier delivery of the particles. The hyaluronan study also shows an accumulation of the particles at the lesion site and minimal delivery in other regions (e.g. the spleen) [40]. For this reason the idea of using NPs as a carrier for anti-inflammatory drugs becomes more plausible.

These particles can be formed by either a top down or bottom up approach. A top down approach starts with big structures and shrinks them back to the nano-scale. This can be achieved with acoustic energy (e.g. sonication) for example. With a bottom up approach the components are put together by force creating the particles. Evaporation techniques are the most commonly used in current nanoparticle fabrication and research (The method is further explained in 2.1.2). What makes this method so popular is the fact that both hydrophobic and hydrophilic drugs can be incorporated in the particle cores. The method is also considered relatively cheap compared to other methods. Another common method, that is a bit more expensive, is using high pressure homogenizing technique (e.g. Herringbone mixer Appendix A) [41]. With high shear stresses, during mixing, the droplets will form in the aqueous solution creating nanoparticles in a pre-emulsion. The smaller the droplets the smaller the particles, this can be controlled by the energy put into the system. Either increasing the temperature or increasing the shear stresses (mixing speed) will decrease the average particle size.

To obtain all the benefits of a NP delivery system there are some design restrictions. The diameter is an adjustable parameter that influences the circulation time of the NPs. Generally speaking particles with a diameter below 100 nm is preferred, however particles with a diameter smaller than 10 nm are easily cleared by kidneys [42]. One of the aims of the research is therefore to obtain particles with a diameter in the range of 10 to 100 nm. The drug delivery is highly correlated with the loading capacity of the NP. Intuitively more particles are needed if the loading capacity is low compared to the number of particles if the loading capacity is high. In order to keep the advantages of the NPs size it is important for them not to aggregate, forming bigger structures by adhering together. Aggregation is highly correlated to the surface potential, since electrostatic repulsion keeps the NPs from coming in close proximity. Surface charge and the medium ionic strength both influence the degree of aggregation [43]. Higher surface potential, which is approximated by the ζ-potential, correspond to a higher stability and usually a greater drug loading efficiency. Drug release profiles also showed to be more gradually when the surface charge is high in magnitude [44]. In the research a ζ-potential of above 30 mV or below -30 mV is considered ideal thus the NP surface charge and the medium have to be adjusted accordingly [45]. Both a medium commonly used in ζ-potentials measurements (HEPES) as well as a medium used for *in vivo* injection experiments (glucose) will be investigated. The incorporation of either cholesterol or biodegradable polymers would improve the stability as mentioned in literature [46].

1.3.3. Aim of the research

The endocannabinoid system, specifically the cannabinoid ligands and receptors, shows promising results in AS therapy. NPs allow for a targeted delivery of this drug. The NP properties and characteristics have a big influence on the performance. The goal of this research is to synthesize and characterize, the physiochemical properties, of different NPs. Additionally the feasibility of the cannabinoid system to use as a target was be evaluated. Finally an *in vitro* investigation would indicate the NPs effect on inflammation. Specifically TNFα and IL-12 will be considered since these are important inflammatory cytokines. The NO production was also be considered since low concentrations correlate with increased cell proliferation while high concentrations correlate with cell arrest and even apoptosis [47].

2

Materials and Methods

In this research the first step should be to synthesize the NPs. The top down and bottom up approach were both used and in total twelve NPs were developed. Their physical and physio-chemical characteristics also had to be evaluated to measure if they meet the requirements for both size, stability and (NPs) yield. Different methods were used and combined to get an all round overview of the characteristics. This was followed by two independent *in vitro* studies. The first focused on the cannabinoid expression, specifically if the CB_2 receptor could be a good target for future research. The second study dealt with the NPs effect on pro-inflammatory cytokine production.

2.1. Preparation of nanoparticles

2.1.1. Materials (used for nanoparticles synthesis)

The following lipid powders: 1,2-dimyristoyl-sn-glycero-3-phosphocholine **(DMPC)**, 1-myristoyl-2-hydroxy-sn-glycero-3-phospho-(1'-rac-glycerol) **(MHPC)** and 1-palmitoyl-2-hexadecyl-sn-glycero-3-phosphocholine **(PHPC)** were purchased from Avanti Polar Lipids (US). 1-palmitoyl-2-oleoyl-sn-glycero-3-phosphocholine **(POPC)** was purchased from Lipoid (US). The primary phospholipids (DMPC and POPC) are observed to be interactive with human ApoA proteins and create proper membranes [48]. Poly (lactic-acid) **(PLA)** and Poly(Lactide-co-Glycolide) **(PLGA)** were purchased from MP Bio (Netherlands) and Sigma Aldrich (US) respectively. Additional details on the lipids and polymers are presented in Appendix B. Apolipoprotein A1 (ApoA1) was purchased from Lee Biosolutions which was extracted from a human donor and stored at 4 °C (US). Cannabidiol **(CBD)** drug powder was purchased from THC Pharm GmbH (Germany). Cholesterol was purchased from Sigma Aldrich (US). All lipid and drug powders as well as the cholesterol were stored at -20 °C. For the top down made NPs the evaporation technique was used in combination with sonication. The MSE Soniprep 150 sonicater (UK) was used for the sonication. For the polymer incorporated particles the high pressure homogenizing method was used. This included two ALADDIN RS232 Syringe Master Pump (US) and a Herringbone mixer of ChipShop (US).

2.1.2. Procedure (used for nanoparticles synthesis)

In Table 2.1 the NPs formulations are summarized for both the top down as well as the bottom-up formulation approaches. NPs made using the top down approach are named NPx with the x being a number from 1 to 4, indicating the 4 primary particles. An additional $x.5$ is used in the labeling when 5mol% cholesterol has been added. For the bottom up derived particles $PGNPx$ or $PLNPx$ is used with PG referring to the incorporation of PLGA and the PL refers to the incorporation of PLA. The x being either 1 or 2, indicating the two different particles. The $\pm$ after the names indicates the presence (+) or absence (-) of the CBD drug. Considering CBD is a well known cannabinoid with promising AS relieving properties, we will use this molecule in our experiments. CBD is also known to be bio-compatible and biodegradable with great affinity to the CB_2 receptor [49].

Traditional synthesis method

For the top down approach the evaporation and sonication techniques were used to synthesize the NPs (Figure 2.1.a). The DMPC, MHPC, PHPC and POPC powders and the CBD drug were dissolved

9

in a 9:1 chloroform/methanol solution before undergoing evaporation under a vacuum, drawing the organic phase out, leaving a dry lipid film, according to the formulations. Subsequently ApoA1 protein was added according to a lipid/ApoA1 weight ratio of 10:1. PBS solution was added up to 2 ml. The aqueous solution together with the lipids, drugs and surfactants were incubated at 37 °C for 3 hours at a shaking speed of 300 rpm. Each sample was then sonicated until the solution became clear. The particles were never sonicated more than 30 minutes. Centrifuging for 10 minutes at 2,500 rpm at 4 °C allowed for the removal of aggregation. The samples were purified from any unincorporated lipid, ApoA1 or drug via centrifugal filtration with a molecular weight cutoff of 100 kiloDalton (Sartorius Stedim Biotech GmbH, Goettingen, Germany). NPs were stored at 4 °C afterwards.
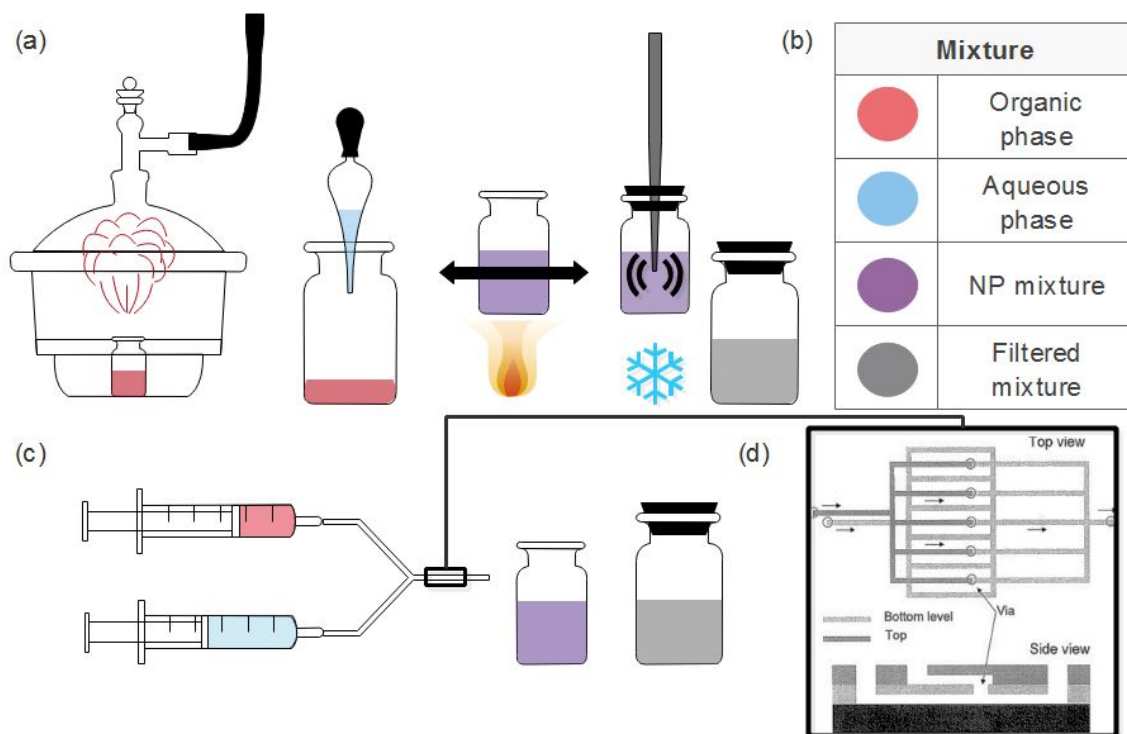

Figure 2.1: **Illustration of the top down and bottom up synthesis method.** (a) The top down approach used for the conventional NPs. The lipid solution, containing the lipids, surfactants (e.g triglyceride and cholesterol) and drugs was mixed with the organic solution (chloroform/methanol). The new mixture will undergo evaporation forming a lipid film. An aqueous solution (ApoA1 and PBS) was added accordingly and mixed. Incubation at 37 °C and shaking for 3 hours before it was sonicated for 10 minutes on ice. Finally a clear solution with the nanoparticles was filtered for aggregation and loose lipids. (b) Color legend showing the organic and aqueous phase together with the mixture and filtered solution. (c) The bottom up approach used for the incorporation of polymers. The lipid solution containing the lipids, polymers, surfactants and drugs was led through the first microchannel at a rate of 3 ml/minute. This was in turn mixed with the aqueous solution (ApoA1 in PBS) which was pushed into a connected microchannel at a rate of 12 ml/minute. The mixture was mixed in the Herringbone mixer and led into a tube containing the NPs solution. Finally a clear solution with the nanoparticles was filtered for aggregation and loose lipids. (d) A top and side view of the Herringbone structure used to mix the two phase provided by [50].

Novel synthesis method: Polymer incorporation

Incorporating the polymers into the formulation required the microfluid channel method, different from the conventional formulations, known as the bottom-up approach (Figure 2.1.c) (n=3). PLA and PLGA powders were dissolved in acetonitrile, while the lipids (DMPC and MHPC with 3:1 molar ratio) and drugs were dissolved in ethanol. The organic solution, with a final volume of 2.1 ml, was mixed in acetonitrile and subsequently injected through one of the Herringbone mixer channels at a rate of 3 ml/minute. In parallel a 8.3 ml ApoA1 solution (0.05 mg/ml diluted in PBS) was injected in another micro-channel at a rate of 12 ml/minute. Via the posterior channel the new mixture could be collected in a glass vial. Centrifuging for 10 minutes at 2,500 rpm at 4 °C allowed for the removal of aggregation using 15 ml tubes. The samples were purified from any unincorporated lipid, ApoA1 or drug via centrifugal filtration with a molecular weight cutoff of 100 kiloDalton. (Sartorius Stedim Biotech GmbH, Goettingen, Germany). NPs were stored at 4 °C afterwards.

Table 2.1: **The composition of the different synthesized nanoparticles.** The names and the general shapes are listed in the first two rows. The NPs can either be empty (**-**) or contain cannabidiol (CBD) (**+**). The primary phospholipids (PL) can be either DMPC or POPC while the secondary phospholipids can be MHPC and PHPC and are added in the mentioned weight ratio's (WR). ApoA1 protein and triglyceride (Tri) are added according to the weight ratio's of the total PL mass. In four cases a polymer is added. Either the PLGA or PLA is added with different weight ratio's to change the size. Cholesterol is added by 5 mol% percentage compared to the PL. In all conditions 26 mass% of CBD can be added, called the loaded NPs (NPx+, PLGAx+ and PLAx+).

General name and shape		Composition					
		Phospholipids			Polymers	Others	
		PL WR	PL : ApoA1 WR	PL : Tri WR	PL : polymer WR	PL : cholesterol mol percentage	PL : CBD mass percentage
NP1±	Disk	DMPC MHPC 9 : 1	10 : 1				26%
NP2±	Sphere	DMPC MHPC 9 : 1	10 : 1	2 : 1			26%
NP3±	Disk	POPC PHPC 9 : 1	10 : 1				26%
NP4±	Sphere	POPC PHPC 9 : 1	10 : 1	2 : 1			26%
NP1.5±	Disk	DMPC MHPC 9 : 1	10 : 1			5%	26%
NP2.5±	Sphere	DMPC MHPC 9 : 1	10 : 1	2 : 1		5%	26%
NP3.5±	Disk	POPC PHPC 9 : 1	10 : 1			5%	26%
NP4.5±	Sphere	POPC PHPC 9 : 1	10 : 1	2 : 1		5%	26%
PGNP1±	Sphere	DMPC MHPC 4,35 : 1	2,5 : 1		PLGA 1 : 2		26%
PGNP2±	Sphere	DMPC MHPC 4,35 : 1	2,5 : 1		PLGA 1 : 10		26%
PLNP1±	Sphere	DMPC MHPC 4,35 : 1	2,5 : 1		PLA 1 : 2		26%
PLNP2±	Sphere	DMPC MHPC 4,35 : 1	2,5 : 1		PLA 1 : 10		26%

2.2. Physiochemical characterization of nanoparticles

The NPs were analyzed with respect to their physical and physiochemical properties i.e. the morphology, size, ζ-potential and protein and phospholipid yield. The protein and phospholipid content indicate the yield obtained by these techniques. The final characteristic of these NPs were the drug entrapment efficiency and loading capacity.

2.2.1. Transmission electron microscopy

TEM images were made using the Philips CM-10 transmission electron microscope (TEM) while confocal images were acquired with the Leica TCS SP8-X confocal microscope. TEM was used for both morphology and size. Briefly, TEM images were obtained using a uranyl acetate negative staining method on copper grids. A drop of a 1:10 dilution of the samples was placed on a paraffin sheet. The copper grids were placed upon the drops for a few minutes before washed three times in water droplets. After each washing step the grids were dried on filter paper. Finally the grids were placed on one uranyl acetate droplet for a couple of minutes before dried again. The sample grids were stored in a petri dish before put into the microscope. The .tiff files were analyzed for NP sizes using ImageJ software.

2.2.2. Size and zeta-potential measurements

Dynamic light scattering (DLS) size measurements and the ζ-potential measurements were performed using the Zetasizer Nano S provided by Malvern (US). DLS measurements were acquired since in the electron microscope the samples are held at dry conditions, which could potentially influence the imaged size. With the DLS the samples were kept in wet conditions. DLS measurements were done with nanoparticles diluted in PBS buffer (ν = 0,8882 and RI (Refractive Index) = 1,334) at 25 °C (n=4). ζ-potential was measured using the Dipp cells at a pH of 7 with the samples diluted in 10 mM HEPES and 10% glucose. For both the drug entrapment efficiency and loading capacity a LC-MS analysis was performed (see section 2.2.4).

2.2.3. Phospholipid and protein characterization

In order to determine the yield of the synthesis methods and the CBD loading a phospholipid assay was performed after filtering. For the phospholipid assay perchloric acid, 1,25% hexa-ammoniummolybdate-solution and 5% ascorbic acid were used and purchased from Sigma (US). A 0,5 mM phosphate solution was used to form the standard curve. Pierce BSA Protein Assay kit was used from Thermo Fisher to determine the ApoA1 yield of the NPs samples (US). The spectrophotometer Perkin Elmer Wallac 1420 Victor2 Microplate Reader was used to measure absorbances, purchased from GMI (US).

A phosphate assay was performed to determine the yield of the phospholipid incorporation into the different formulations. We speculate that a higher phospholipid yield indicates the formation of more NPs. To normalize the cell *in vitro* treatments, this yield difference is taken into account. It is also used to calculate the CBD yield. Briefly, a standard curve containing 0, 40, 60, 80, 100, 120 and 160 μL of the 0,5 mM phosphate solution (KH_2PO_4) was prepared. 100 μL of each NPs sample was added to two glass tubes (n=3). The samples were placed in a heating block for 45 minutes at 190 °C to completely dry the phospholipids, followed by the addition of 300 μL of perchloric acid. Afterwards they were placed in the heating block for 1 hour while covered with a glass marble on top (to trap the evaporating mixture). Cooling the tubes down to room temperature before 1 ml of MiliQ water, 400 μL of 1,25% hexa-ammoniummolybdate solution and 400 μL of fresh made 5% ascorbic acid were added. For 5 minutes the tubes were placed in a boiling water bath before cooled down again to room temperature. The absorbance of each sample was measured at a wavelength of 797 nm using the spectrophotometer Microplate Reader.

For the protein assay the Bicinchoninic acid (BCA) kit was used in order to determine the ApoA1 yield of synthesized NPs (n=3). Briefly, albumin-based standards were diluted, in the range of 25 up to 2000 μg/ml. A working reagent was mixed using a 50:1 volume ratio of reagents A and B respectively. In a well plate, 25 μL of each standard and sample was pipetted in duplo. 200 μL of working reagent was added to each well and properly mixed for 30 seconds. Afterwards, the plate was covered and incubated at 37 °C for 30 minutes. The absorbance was measured at 562 nm using the spectrophotometer Microplate Reader.

2.2.4. Drug loading

Chromatography data was obtained using a Liquid chromatography–mass spectrometry (LC-MS) and used to determine the drug loading efficiency of the particles. LC-MS was used because of it ability to combine the separation of a mixture properties of liquid chromatography and the structural identification virtue of mass spectrometry. The first feature is mostly important since we work with multiple components in our formulation. While the second feature allows for the identification of the CBD. A 10μM CBD diluted in ethanol was sent beforehand to be used as an identifier mass. An empty NP sample was prepared and different concentrations of CBD was added to these formulations after filtering to work as a calibration curve for the loaded samples. These different concentrations were in the range of 0 to 10 μM and were measured without the company knowing beforehand the concentrations (n=2). The results were later compared to the expected results and the technique was validated. Finally the samples were sent, measured and the results were communicated back (n=1). Although the theoretical knowledge of LC-MS is known, we were unable to see or perform the measurements ourselves.

The drug loading capacity indicates the weight of the NPs that is attributed to the drug. Likewise the entrapment efficiency indicates the amount of which the drug is incorporated in the NPs, also called yield. The loading content and entrapment efficiency were calculated using the following equations:

$$Drug \quad loading \quad content(\%) = \frac{Weight \quad of \quad drug \quad in \quad NPs}{Weight \quad of \quad NPs} * 100$$

$$Entrapment \quad efficiency(\%) = \frac{Weight \quad of \quad drug \quad in \quad NPs}{Weight \quad of \quad drug \quad input} * 100$$

In order to calculate the above equations the phospholipid yield had to be known as well. Limited time did not for polymer incorporated NPs to be measured for their drug loading content and entrapment efficiency.

2.3. Cannabinoid receptor expression

2.3.1. Cell culturing on paraffin sections

The 57BL/6 mouse naive cells were plated on 24 well plates and kept in preheated 37 °C Phosphate-buffered saline buffer (PBS) medium for 4 hours. Either 50 μg/ml of ox-LDL or Acetyl-LDL or regular medium was added to mimic AS conditions as well as create a control group (regular medium). A 1:10 dilution of the recombinant Murine cytokines was added and the cells were incubating for 24 hours to create a pro- and anti-inflammatory condition. Only additional PBS medium was added to the control groups. For the confocal microscopy imaging the paraffin sections were used.

2.3.2. Cell and receptor staining on single cells

For the cannabinoid expression study naive C57BL/6 mouse macrophages were sacrificed after 8 weeks. Lipopolysaccharide (LPS) was purchased from Sigma Aldrich (US). Recombinant Murine IL-4 (10 ng/ml) used for the anti-inflammatory stimulus was obtained from Peprotech (Netherlands). For the pro-inflammatory conditions 100 U/ml recombinant Murine Interferon gamma (IFNγ) was purchased from Hycult BioTechnology (Netherlands). The agents were kept on ice until use. A preheated (sterile) RPMI-1640 medium (containing 10% Fetal bovine serum (FBS), 100 U/ml penicillin, 100 μg/ml streptomycin, 2mM L-glutamine and 10mM HEPES) was prepared beforehand in the lab and stored at 4 °C up until use. For the immunoflorescence staining paraffin sections were used. Xylene, 100% and 95% ethanol were used to deparaffinize and hydrate the sections (n=2). PBS and PBS with 0.02% Tween are stored at room temperature while antigen buffer was kept at 4 °C. Blocking solution was made fresh with PBS and 10%FBS. The primary antibodies were ordered from TOCRIS, specifically CB_1 antigen with rabbit host and rat target and CB_2 antigen with rabbit host and human target. The CB_1 antibody has been kept at -20 °C while the CB_2 antibody has been kept at 4 °C. Alexa Fluor 647 donkey host and rabbit target was the secondary antibody used for both antibodies and was purchased from Thermo Fisher (US). It ought to be stored in the dark at 4 °C up until use. For nuclei staining the 4,6-Diamidino-2-Phenylindole (DAPI) which can bind to AT regions of the DNA was used. Anti fade mounting media was purchased from Thermo Fisher used to limit fluorescence loss between the preparation and the imaging (US).

Paraffin sections of aortic plaque lesions were obtained from an ApoE$^{-/-}$ mouse that was put on a high fat diet for 12 weeks. The mouse would have developed AS up around stage 5. Briefly, the sections were deparaffinized in xylene. Hydration followed using ethanol baths. The sections were rinsed before washed in PBS. The sections were put in a boiling antigen retrieval buffer bath before washed again. The sections were incubated in blocking solution for 1 hour. A 1:200 dilution of the antibodies in blocking solution was added to the sections followed by the incubation at 4 °C for 24 hours. The sections were washed before the secondary antibody was added (diluted 1:500) for another hour. After washing a 2 g/ml diluted DAPI was incubating for 15 minutes. Finally the sections were washed before mounted with anti fade media.

2.4. *In vitro* nanoparticles techniques

2.4.1. Cell culturing for *in vitro* experiments

8 weeks old wild type C57BC mice put on a regular diet were sacrificed for culturing of macrophages from the bone marrow. PBS and citrate solution were stored at 4 °C up until use. RPMI-1640 was prepared beforehand in the lab by the AMC department and stored at 4 °C up until use. All were bought from Thermo Fisher Scientific (US). Cells were counted using the CASY TTC Cell counter analyzer. This was purchased from OMNI Life Sciences (Germany) and can measure viable cells in a 20 μL of cell suspension. To induce macrophage differentiation, L929 conditioned medium (LCM) containing macrophage-colony stimulating factor (M-CSF) was used. Briefly, the LCM was extracted from the cultured L929 mouse cell line medium. The medium contained M-CSF which promotes macrophage differentiation from monocytes. This was provided by the AMC department and had to be stored at -20 °C until use. Acetylated LDL (Acetyl-LDL) from human plasma was used for the foam cell formation and was purchased from Thermo Fisher Scientific (US).

2.4.2. Incubating cells with nanoparticles

Monocytes derived from wild type C57BL/6 mice were cultured in the culture medium RPMI-1640 with 15% LCM and incubated at 37 °C with a 5% CO_2 atmosphere for 9 days. After 72 and 144 hours RPMI-1640 with 15% LCM was added and refreshed both to differentiate the cells and to keep them alive. LPS and IFNγ were added to induce pro-inflammatory macrophages. On the 9th day the cells were cultured and detached using a 0.2 μM citrate solution. After 5 minutes of incubation a RPMI-1460 medium (without LCM) was added inactivating the citrate solution. Cells were counted using the CASY TCC and distributed over either 24 or 96 well plates (200,000 and 500,000 per well plate respectively). For 24 hours the NPs were incubated with the cells. For medium isolation the plates were centrifuged allowing the cells to spin down while the medium remains above. The medium was transferred into a new well plate and stored at -20 °C for further experiments.

2.4.3. ELISA on cytokines

The protein concentration for both TNFα and IL-12 were determined using the Enzyme-Linked Immuno Sorbent Assay (ELISA). The Life Technology antibody pair kits CMC3013 and CM0063, containing the capture and detecting antibodies as well as the working conjugator, were used for the both TNFα and IL-12 respectively and were purchased from ThermoFisher Scientific (US). The chromogenic substrate 1-Step^{TM} Ultra TMB-ELISA Substrate Solution (TMB), purchased from Thermofished Scientific, was used for the optical density measurement (US). TMB was stored at 4 °C in the dark until use. A PBS solution containing 0.5% BSA and 5% FCS was used for sample dilution, while the block buffer was merely a PBS solution with 0.5%BSA. For the washing of the plates a wash buffer containing 0.05% Tween in PBS was made. 1,8M H_2SO_4 in water was used for the stop solution. The standard used for the calibration curve was stored at -80 °C. Measurements were done using optical density of the well at 450 nm using the Perkin Elmer Wallac 1420 Victor2 Microplate Reader (US).

For both the TNFα and IL-12 protein expression two Maxisorp 96 flat-bottom well plates (Thermo Fisher) were coated with the capture antibody and kept overnight at 4 °C. The plates were blocked using the block buffer for 2 hours while kept sealed at room temperature. For the TNFα a 1:10 dilution of the samples and the standard were added to the wells before sealed for 1 hour at room temperature in the dark. For the IL-12 assay there was a 1:20 dilution used and kept under the same conditions. The detector antibodies were added to the wells diluted 1:2000 for TNFα and 1:4000 for IL-12, respectively before kept at room temperature in the dark for 1 hour. In both assays the plates were washed twice

using the wash buffer. For the third incubation a 1:1500 and a 1:5000 Streptavidin-HRP dilution of the working buffer was added for TNFα and IL-12 respectively. The plates were again kept in the dark at room temperature for another hour. For both assays the plates were washed four times with the wash buffer, before 50 μL TMB was added to each well. The color will develop and therefore the plates were kept in the dark. When the color developed enough the stop solution was added to the wells. The optical density was measured at 450 nm for both protein assays using the spectrophotometer Microplate Reader. With the standard dilutions a calibration curve was made for further analysis.

2.4.4. Cytotoxicity experiment

The production of NO could be measured using a Griess reaction. 2mM $NaNO_2$ and Griess reagent solutions (stored at 4 °C) were used in this experiment. Griess reagents consisits of water with 2.5% H_3PO_4, 1% sulfanilamide and 0.1% naphtylene diamine dihydrochloride. Naphtylene diamine dihydrochloride was purchased from Sigma (US). Measurements were done using optical density of the well at 548 nm using the Perkin Elmer Wallac 1420 Victor2 Microplate Reader (US). For the NO assay 50 μL of the samples was transferred to a new well plate. The standard dilution, based on the $NaNO_2$, was used to make a series of concentrations, ranging from 3,125 up to 200 μM, in order to calibrate the measurements. 50 μL of Griess reagent was added to each sample and the each standard. The absorbances were measured using the spectrophotometer at 550 nm.

2.5. Statistical analysis

The results will be presented with the average $\pm$ SD. In case of two groups the unpaired two tailed t-test was used. For more groups a one-way ANOVA tests was used. Both statistical analyses were performed using GraphPad Prism 4.0. P<0.05 was regarded as significant.

3

Results

3.1. Synthesis and physio-chemical characterization of nanoparticles

3.1.1. Size distribution and morphology

In order to study the influence of the formulation on size, stability and morphology the DLS measurements and a few selected dry TEM images are presented in Figure 3.1. These TEM images were selected in order to illustrate the different formulation groups, the empty, loaded and cholesterol incorporated NPs. The first noticeable behavior, by comparing the different particles at zero days, is the increased size of the NPs when 5 mol% cholesterol is added (P<0.0001) (Figure 3.1). This trend is seen in all formulations except for the NP4 samples (P>0.05). It is also striking to note that adding cholesterol does influence the stability over time (30 days), again the NP4 samples do not agree with this observation. Adding the CBD drug (26 mol%) does not increase the NP size significantly only in the case of NP4. Interestingly the NP size does not further increase when cholesterol is added to this particular formulation (P>0.05). Overall the samples without cholesterol, regardless of drug loading, remain of similar size even after a month.

Furthermore the use of other phospholipids (POPC and PHPC in contrast to DMPC and MHPC) does not affect the size considerably. The addition of triglyceride (NP2 and NP4) does also not alter the size significantly. However the shape does shift from a disk shape to a more spherical shape as presented in Figure 3.1b when comparing NP1- and NP2+. It is important to note that this is not influenced by the drug loading, since NP2- particles show a similar shape. When comparing the NP images to the ApoA1 control image it can be presumed that the structures are indeed nanoparticles and not background noise. NP3.5+ TEM images showed a structure similar to a collapsed sphere, this will be further explored in the discussion section.

For the PLA and PLGA incorporation both DLS measurements and TEM images were made. Their size, stability and morphology were analyzed and summarized in Figure 3.2. From the TEM images the NP sizes could be extracted using ImageJ software which are presented next to the DLS measurements in Figure 3.2a. No considerable difference could be found between the DLS and TEM (P>0.05), which could indicate that the measured size is the actual size. This was also observed with the same samples after 30 days. The 4 samples were all spherical as shown in Figure 3.2b. The formulations with a higher polymer to phospholipid ratio (PGNP2 and PLNP2) seemed to be bigger than the other two formulations. That aside, using one of these polymers over the other does not significantly alter the size or morphology.
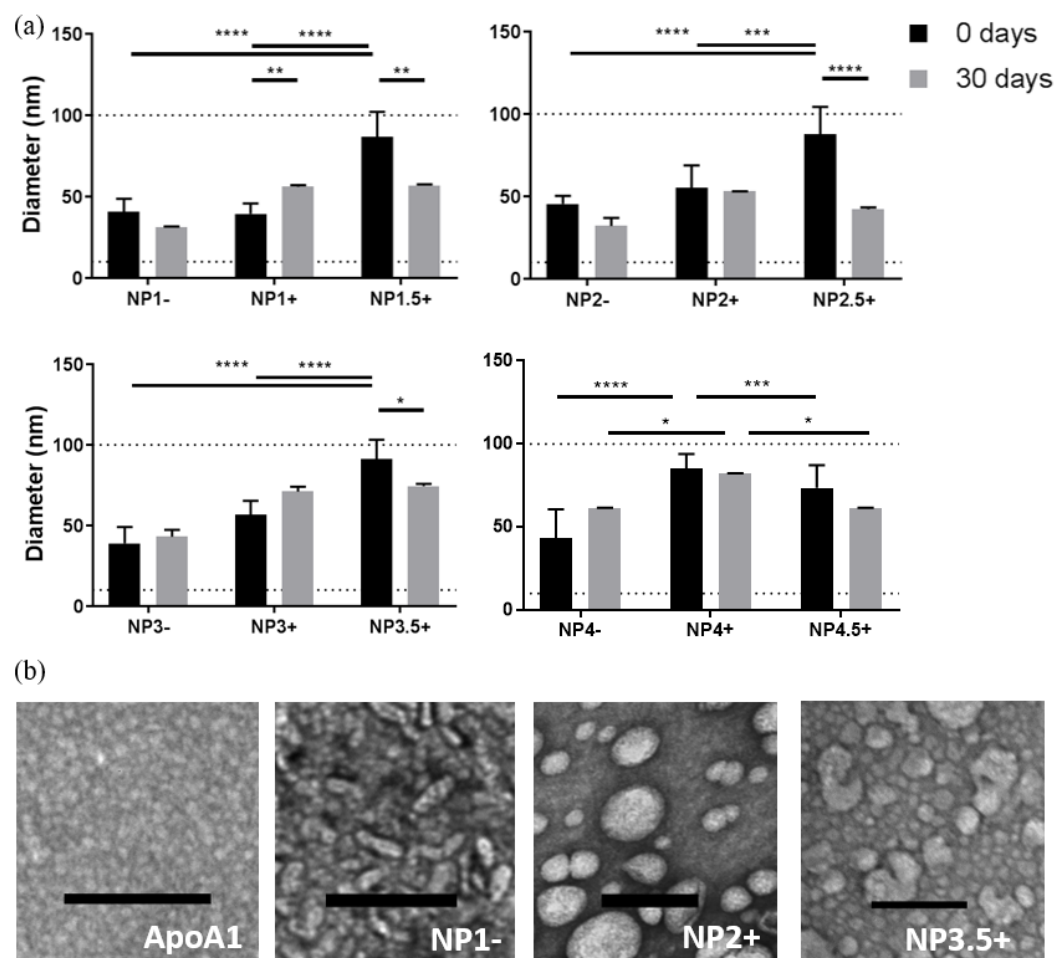
Figure 3.1: **Diameter of NPs measured using the dynamic light scattering technique and TEM (n=4)**. (a) The diameter of the NPs synthesized using the top down approach after filtering and after 30 days. In between measurements the NPs were stored at 4 °C in a PBS buffer. Settings were set on $\nu = 0,8882$ and RI (Refractive Index) = 1,334 at 25 °C and measurements were done in disposable cuvettes. The dotted lines represent the range in which the particles have to remain (10 to 100 nm in diameters). Error bars are SDs. Statistics was calculated with the one-way ANOVA test. Statistically significant of P<0.05, P<0.01, P<0.001 and P<0.0001 are annotated with *, **, *** and **** respectively. (b) TEM acquired images of different types of NPs (scale bar = 100 nm). The control image (ApoA1) shows the background signal that present in the other conditions. TEM images were made between 0 and 14 days after synthesis.

3.1.2. Surface charges of nanoparticles

The ζ-potential is an indication for the stability of particles in a solution and is dependent on the particle surface charge and the ionic strength of the medium. In Figure 3.3 the ζ-potentials for two different buffers are presented. The first one being HEPES, a commonly used buffer for measurements and a glucose medium, which can be used as injection medium for *in vivo* experiments, maybe in the future. Additionally a buffer with known ζ-potential in 10 μM HEPES was measured as well. Figure 3.3 shows that the ζ-potential is negative in both buffers which is considered to be non-toxic for cells. However the ζ-potential's magnitude should ideally be above 30 mV, to limit aggregation, which is not the case. Only the NP1- touches this threshold lightly when in HEPES. Overall the addition of CBD or cholesterol does not influence the ζ-potential, except for NP1 and NP1 with 5mol% cholesterol in which cases the ζ-potential decreases (P<0.0001). Additionally the ζ-potential was measured in 5% glucose (Figure 3.3b). In contrast to the expectations the ζ-potential decreases or remains similar. NP4+ samples also seem to cover positive values, which is not desirable (MEAN = -1,03 SD= 9,67 mV). Because of limited stock the particles with cholesterol were not measured in 5% glucose. The theoretical ζ-potential (MEAN= 42.0 SD= 4.8 mV) was in agreement with the 10 μM HEPES measurements and did not drastically change due to the 5% glucose buffer (Figure 3.3c).
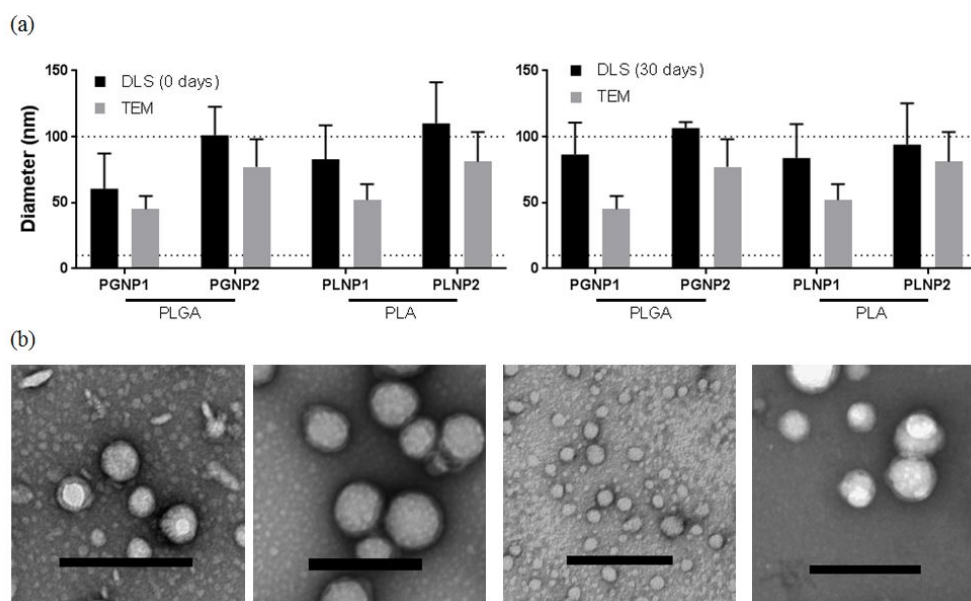
Figure 3.2: **Diameter of empty NPs, with incorporated polymers, measured using the dynamic light scattering technique and TEM (n=4)**. (a) The diameter of the NPs synthesized using the bottom up approach after filtering (left) and 30 days (right). DLS measurements were acquired using ν = 0,8882 and RI = 1,334 at 25 °C. The dotted lines represent the range in which the particles have to remain (10 to 100 nm in diameters). Using the ImageJ software the diameter was measured from the TEM images. Error bars are SDs. Statistics was calculated with the one-way ANOVA test. (b) TEM acquired images of different types of empty NPs (scale bar = 200 nm). TEM images were made between 0 and 10 days after synthesis of PLGNP1-, PLGNP2-, PLNP1- and PLNP2- in order.
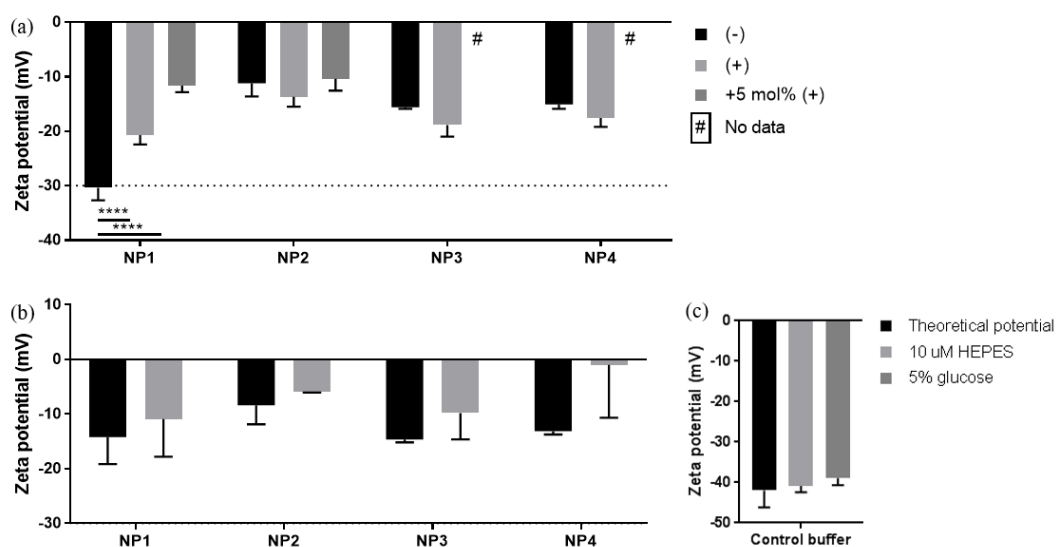

Figure 3.3: ζ-**potential measurements of NPs diluted in 10 μM HEPES buffer and 5% glucose (n=3)**. (a) The NPs were measured in a 10 μM HEPES buffer at a constant pH of 7 in Dipp cells. The dotted line (-30mV) represents the ζ-potential threshold required for stable particles. # indicates that sample was not analyzed for the ζ-potential. Two samples could not be measured due to limited material. (b) The NPs were measured in a 5% glucose solution at a constant pH of 7 in Dipp cells. The dielectric constant for the medium was set on 90. Error bars are SDs. Statistics was calculated with the one-way ANOVA test. Statistically significant of P < 0.0001 is annotated with ****. (c) The control buffer is known to have a ζ-potential of -42.0 ± 4.2 mV in 10 μM HEPES and 5% glucose.

3.1.3. Protein and phospholipid yield assays

The method used to synthesize these particles consists of several steps, it is thus not uncommon for materials to get lost. In Figure 3.4 the calibration curve, used to determine the concentration, the measured and known stock concentration, of the ApoA1 protein, and the NP sample results are

presented. Firstly the calibration curve shows an adequate regression of the date with limited variance between the samples. In Figure 3.4b the 5 and 10 times diluted samples do show a similar concentration as the theoretical sample. However, in Figure 3.4c, it is clear for the NP samples, the output signal is higher than the protein input (dotted line). This makes the method unsuitable for measuring the protein concentration of HDLs. A similar experiment based on the DC protein assay was performed showing interference of the particles as well (Appendix C). Comparing NP1± and NP2± shows that the adding CBD could increase the yield (by inter-sample comparison). Nonetheless no sound observations can be extracted from the results.

In Figure 3.5 the calibration curve for the phospholipid assay and the NP sample results are summarized. The calibration curve does show a competent regression of the data. Because the phospholipid input for each sample is different, the data in Figure 3.5b is presented as the yield%. No significant difference could be found between empty and loaded particles. The variability between samples is also relatively small, leading us to suspect that the yield is relatively consistent and does not vary between sample preparations. The phospholipid yield could be an indication of the amount of successfully formed NPs. Therefore these samples are diluted accordingly so that the final concentration of phospholipids is the same (1, 5 and 10 μM).
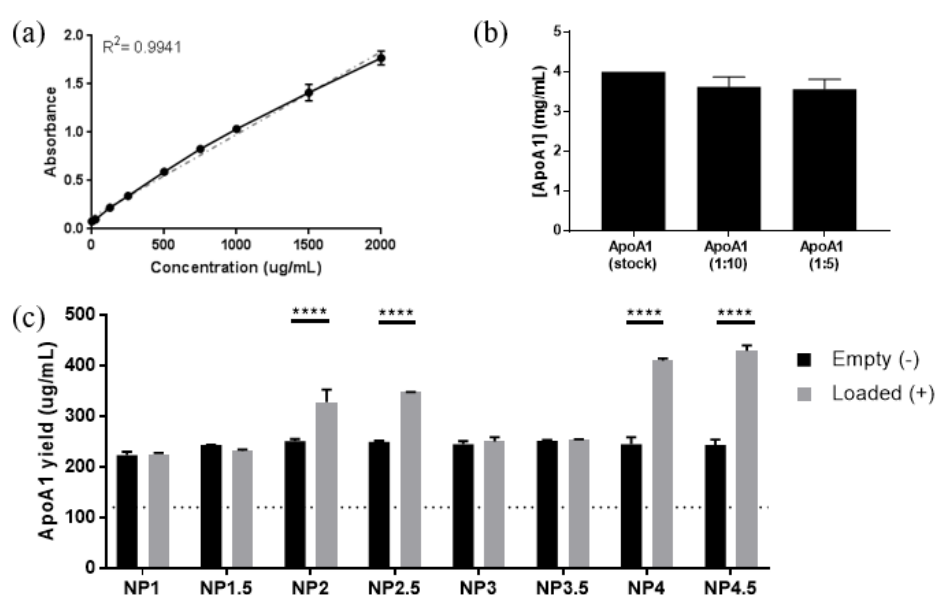

Figure 3.4: **Protein concentration measurements for the NPs after synthesis based on the BCA protein assay (n=3)**. (a) The calibration curve (black) shows a linear regression of 0.9941 (grey dotted line) which allows for proper analysis of the samples. With the x- and y-axis being the concentration and absorbance respectively. (b) As a control the protein stock with known concentration (4 mg/mL) was measured in a 1:10 and 1:5 dilution. The measurements are within the range of expectation. (c) The dotted line represents the ApoA1 input for the empty (-) and loaded (+) NPs. Error bars are SDs. Statistics was calculated with the unpaired t test. Statistically significant of P <0.0001 is annotated with ****.

3.1.4. Cannabidiol drug loading efficiency

Table 3.1 shows the entrapment and loading of CBD in the four different formulations (without cholesterol and polymers). The first thing that can be seen is that the loading is below 50% for all samples. The NP1 sample has the greatest incorporation efficiency while NP4 has the lowest. Because it was only possible to measure one sample no statistical analysis could be performed. The calibration curve for the CBD was not incorporated in the body of the thesis since only a graph was provided by the company. This graph is however presented in Appendix D and shows a desired linear relationship between the signal and concentration.
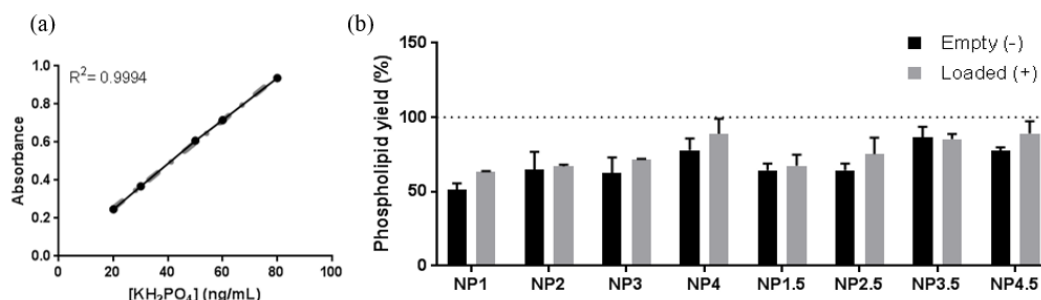
(a)

(b)

Figure 3.5: **Phospholipid yield after NP synthesis and filtering (n=3).** (a) The calibration curve (black) shows a linear regression of 0.9994 (grey dotted line) which allows for proper analysis of the samples. With the x- and y-axis being the concentration and absorbance respectively. (b) The yield percentage is calculated using the input and normalized (dotted line at 100%) to allow for a better comparison between the samples. Error bars are SDs. Statistics was calculated with the unpaired t test.

Table 3.1: **CBD entrapment and incorporation efficiency (n=1).** With the LC-MS technique and the equations presented in section 2.2.4 the following results were obtained. No statistical analysis test could be applied.

Sample	CBD entrapment efficiency (%)	Loading content (%)
NP1	26,66	41,82
NP2	24,16	36,03
NP3	25,98	36,28
NP4	18,55	20,87

3.2. Receptor expression in mimicked atherosclerotic conditions

3.2.1. Cannabinoid receptor expression of single cells

The Figures 3.6 and 3.7 present the CB_1 and CB_2 receptor expression (green), respectively, in different inflammatory conditions. The cell nuclei (blue) show the location of the macrophages and allows for cell counting. The traditional anti-inflammatory conditions (upper left) and the traditional pro-inflammatory conditions (lower right) show a difference in both the signal and cell clustering. Anti-inflammatory conditions (IL-4 stimulated cells) show a relatively weak signal of the receptors as well as scattering of cells. The addition of anti-inflammatory (IL-4) and an inherently pro-inflammatory (Acetyl-LDL) stimulus does decrease the CB_2 expression but does little to CB_1. The control macrophages (upper middle) do not significantly differ in CB_1 and CB_2 expression. Interestingly adding only Acetyl-LDL (lower middle) does not seem to be enough for CB_1 and CB_2 receptor over-expression. Adding LPS and IFNγ (upper right) does show the clustering associated with pro-inflammatory macrophages. The packed macrophages also progress into the z-direction (orthogonal to the picture) which is indicated by unfocused and focused areas in these images. It can be seen that combining LPS, IFNγ and Acetyl-LDL increases the CB_1 and CB_2 expression, regardless of cell density (lower right). Because these experiments were done separately the CB_1 expression cannot be compared to CB_2 receptor expression.

3.2.2. Cannabinoid receptor specificity to macrophages investigation

The macrophages (green), cell nuclei (blue) and CB_1 and CB_2 receptors (red) were stained in an AS plaque lesion as shown in Figure 3.8. The four left images are part of the same plaque section and stained for CB_1, while the right images are part of a different plaque section and stained for CB_2. The overlay of the different fluorescence signals is shown in the lower second and fourth images. As expected not all cell nuclei belong to the macrophages, since endothelial cells, smooth muscle cells and other leukocytes are also known to be located in the plaque. Nonetheless the macrophages do take up a large volume of the lesion. The CB_1 is observed to co-localize with the macrophages (e.g. white arrows). Either background noise or aspecific antibody binding could explain the non-macrophage CB_1 signal. The observations for CB_1 can also be seen for CB_2 expression. The necrotic cores (red arrows) do show limited macrophage and CB_2 staining, CB_1 antibodies seemed to have leaked in necrotic cores. This is an indication of an abundance of CB_1 antibodies. Nonetheless both antibodies seem to be specific to localize the receptors.
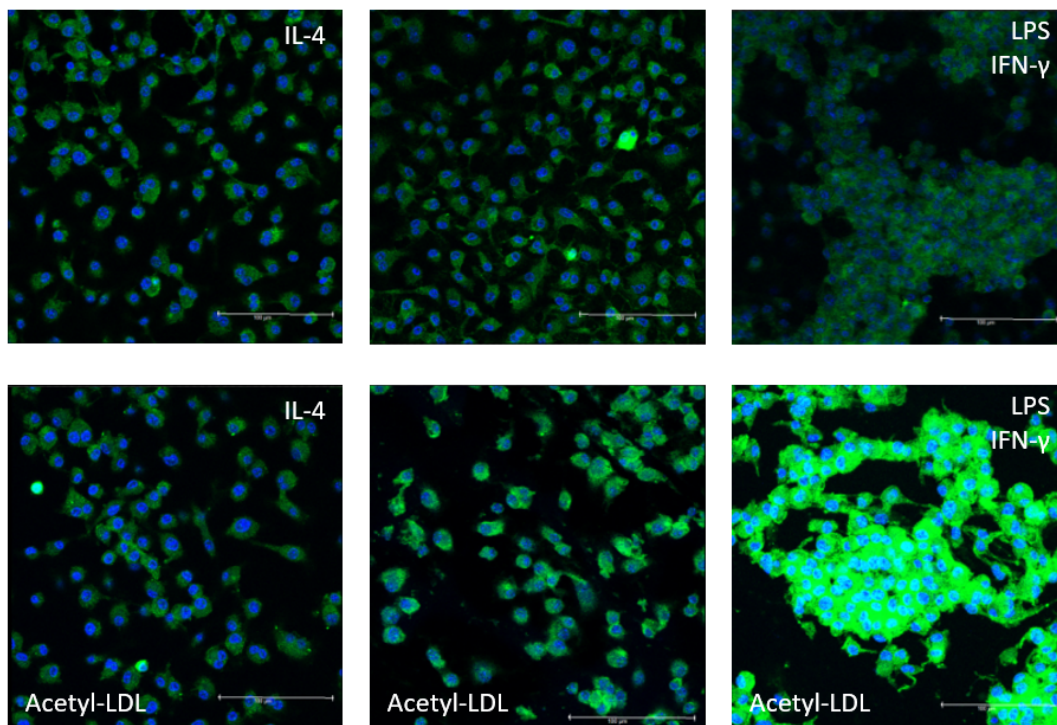
Figure 3.6: CB_1 **receptor expression in different macrophage types (scale bar = 100 nm).** Cell nuclei stained with DAPI (blue) and CB_1 receptors stained with CB_1 antibodies (green). Upper left image shows macrophages stimulated with only IL-4, an anti-inflammatory cytokine, while the upper middle image shows naive macrophages. Upper right image shows macrophages stimulated with LPS and IFN-γ simulating pro-inflammatory conditions. The bottom images present the same conditions as the upper ones however an additional Acetylated LDL is added as well, creating foam cells.
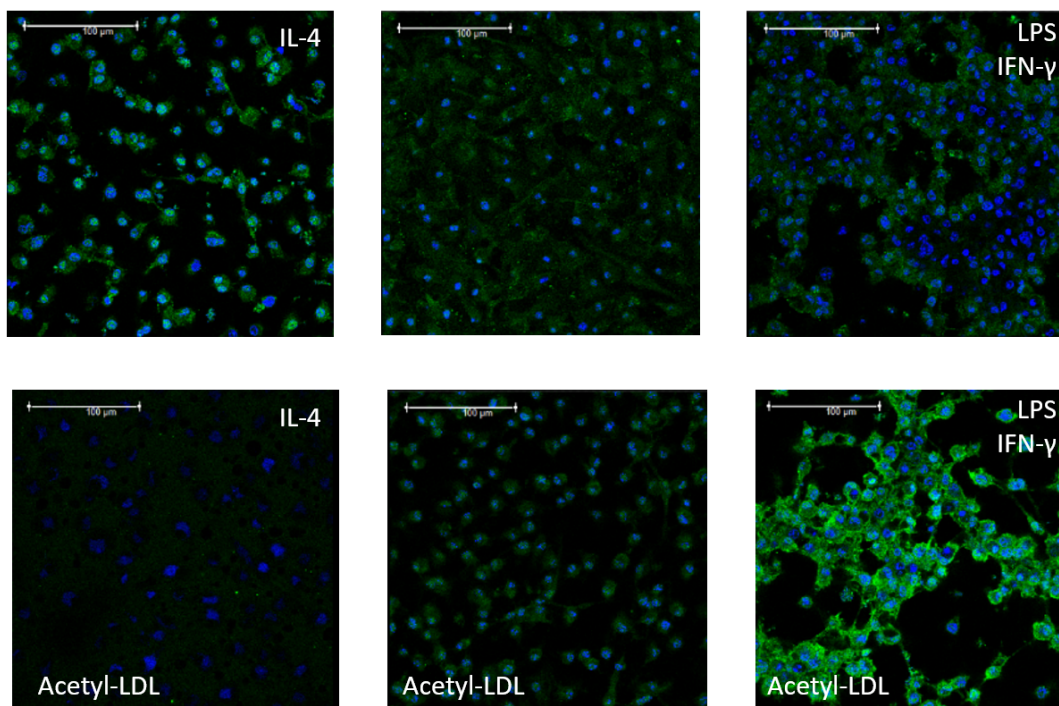

Figure 3.7: CB_2 **receptor expression in different macrophage types (scale bar = 100 nm).** Cell nuclei stained with DAPI (blue) and CB_2 receptors stained with CB_2 antibodies (green). Upper left image shows macrophages stimulated with only IL-4, an anti-inflammatory cytokine, while the upper middle image shows naive macrophages. Upper right image shows macrophages stimulated with LPS and IFN-γ simulating pro-inflammatory conditions. The bottom images present the same conditions as the upper ones however an additional Acetylated LDL is added as well, creating foam cells.
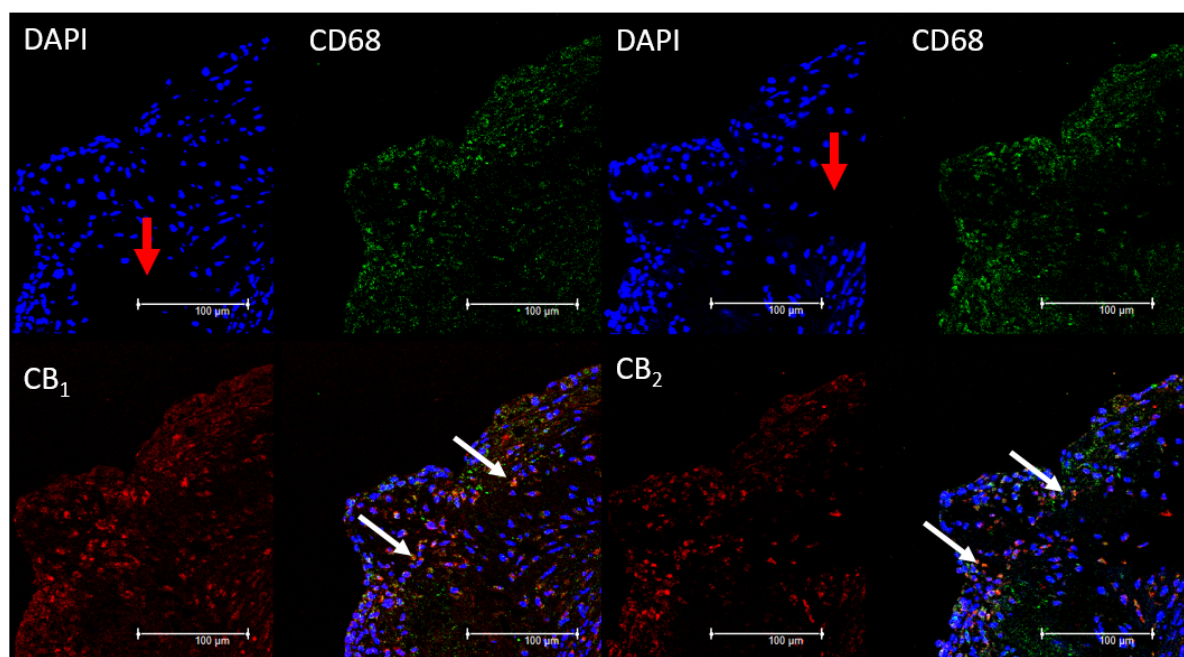
Figure 3.8: **Confocal fluorescence microscopy images of plaque sections (scale bar = 100 nm).** The two left upper and down images show a single sections which was stained for cell nuclei, using DAPI, (blue) macrophages, using CD68 antibodies, (green) and CB_1 receptors, using CB_1 antibodies, (red). These three images were stacked in the second image in the bottom row. The two right upper and down images show a similar staining of another sections however with the CB_2 receptor stained using CB_2 antibodies (red). White arrows indicate a few examples of co-localization of CD68 with either CB_1 or CB_2. Red arrows indicate examples of necrotic cores.

3.3. *In vitro* assessment

3.3.1. Nanoparticles treatment effect on Nitric Oxide

In Figure 3.9 the NO concentration of the controls and the NP treated samples are plotted for three different concentrations. Since PBS is the medium in which the particles are kept this is a clear control group. Also, by adding 10 μM of CBD the single effect of CBD can be analyzed. Because CBD has to be diluted in ethanol a third control was needed to take this into account (EtOH). When comparing the different controls to each other it can be seen that 10 μM CBD does not influence the NO concentration substantially (Figure 3.9). The added ethanol does not have a big impact as well.

Comparing the different types of NPs and the different concentrations a couple of things can be noted. For the empty and loaded NP2 samples there has been a significant difference found between 1 and 10 μM. For NP2.5, NP3 and NP4.5 a significant decrease could be observed between the loaded 1 and 10 μM samples (P<0.05). Interestingly, 5 μM of NP1.5 is seen to be decreasing the NO concentration compared to 1 and 10 μM. Both NP1 and NP4 do not show significant effect of NPs concentrations on the NO (P>0.05). Finally the NP3.5 samples show interesting results. Adding either 5 and 10 μM of empty NPs show a decreased NO concentration when compared to 1 μM (P<0.05). There is also a decrease between the loaded samples, namely 10 μM shows a drop in NO compared to 1 μM (P<0.0001).

Some individual sample groups showed some behavior worth discussing. Firstly, both NP1 and NP2 show a considerable drop in NO in the loaded samples compared to the empty samples, specifically for 5 and 10 μM treatments (P<0.05). The loaded NP4 samples shows however an increase in NO compared to the empty samples. This is however only the case for 1 and 10 μM. The most compelling differences could be found in the NP3.5 samples. For each concentration measured, the loaded NPs decreased the NO concentration considerably, compared to the empty samples. In Figure 3.10 the samples with a significant decrease in NO concentration are summarized. The empty NP4 samples seem to decrease the NO in all measured conditions (P<0.01). The samples with cholesterol do seem to also decrease the NO concentration when added in higher concentration (e.g. NP1.5, NP2.5 and NP4.5).
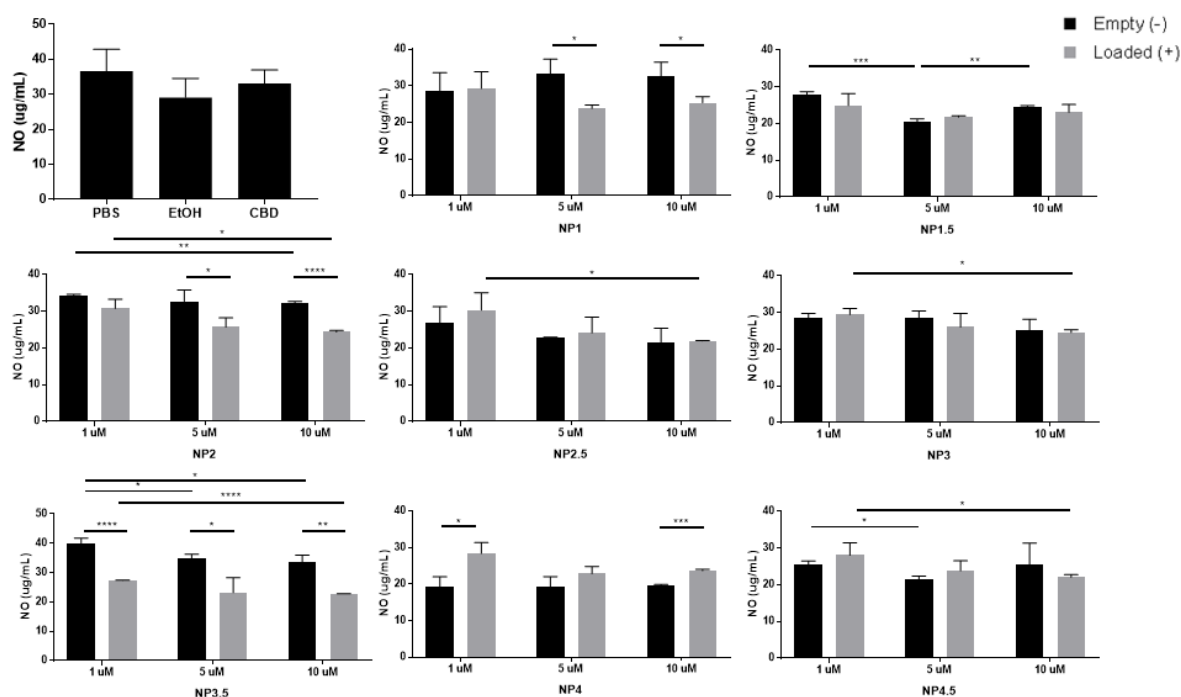
Figure 3.9: **NO concentration measurements after 24h incubation of NPs diluted in PBS (n=3)**. The upper left graph show the NO concentration of the control groups with 10 μM ethanol and CBD. The other graphs compare the empty (black) and loaded (grey) NPs added in three different concentrations. Error bars are SDs. Statistics was calculated with the two way student t-test. Statistically significant of P<0.05, P<0.01, P<0.001 and 0.0001 are annotated with *, **, *** and **** respectively.
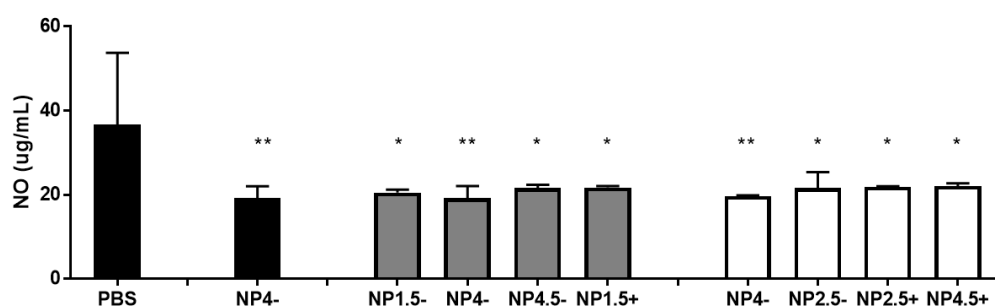

Figure 3.10: **Significant decreased NO concentration in NPs treated samples (n=3).** Each samples was compared to the PBS control group and the significantly different treatments are summarized in this figure. Black bars indicate the 1 μM added conditions, grey bars indicate 5 μM and white bars indicate the 10 μM. Error bars are SDs. Statistics was calculated with the two way student t-test. Statistically significant of P<0.05 and P<0.01 are annotated with * and ** respectively.

3.3.2. Cytokine assay after nanoparticles treatment

In Figure 3.11 the TNFα concentration of the different conditions are summarized. Again the PBS, ethanol and CBD treatments are the control groups for the same reason as for the NO assay. The TNFα production does however remain in most cases unchanged. Both the CBD and ethanol do not decrease the concentration enough to be considered significant (P>0.05). Also limited differences could be found between the loaded and empty particles. The times a difference occurs however the loaded particles perform worse than the empty particles. Figure 3.12 presents the different treatments that show a significance decline in TNFα production when compared to PBS. The NPs with cholesterol are the majority in this graph. NP3.5 shows decreasing TNFα production in all measured concentrations. Interesting to note it that the 10 μM CBD treatment (control group) did not decrease the TNFα production. It is therefore possible to speculate that the drop we measure in the samples is due to the HDL particle itself. This is further supported by the fact that the loaded samples do not perform better.

Finally, a statistical analysis between the NPs and the 10 μM CBD control group was performed, no significant difference was found.
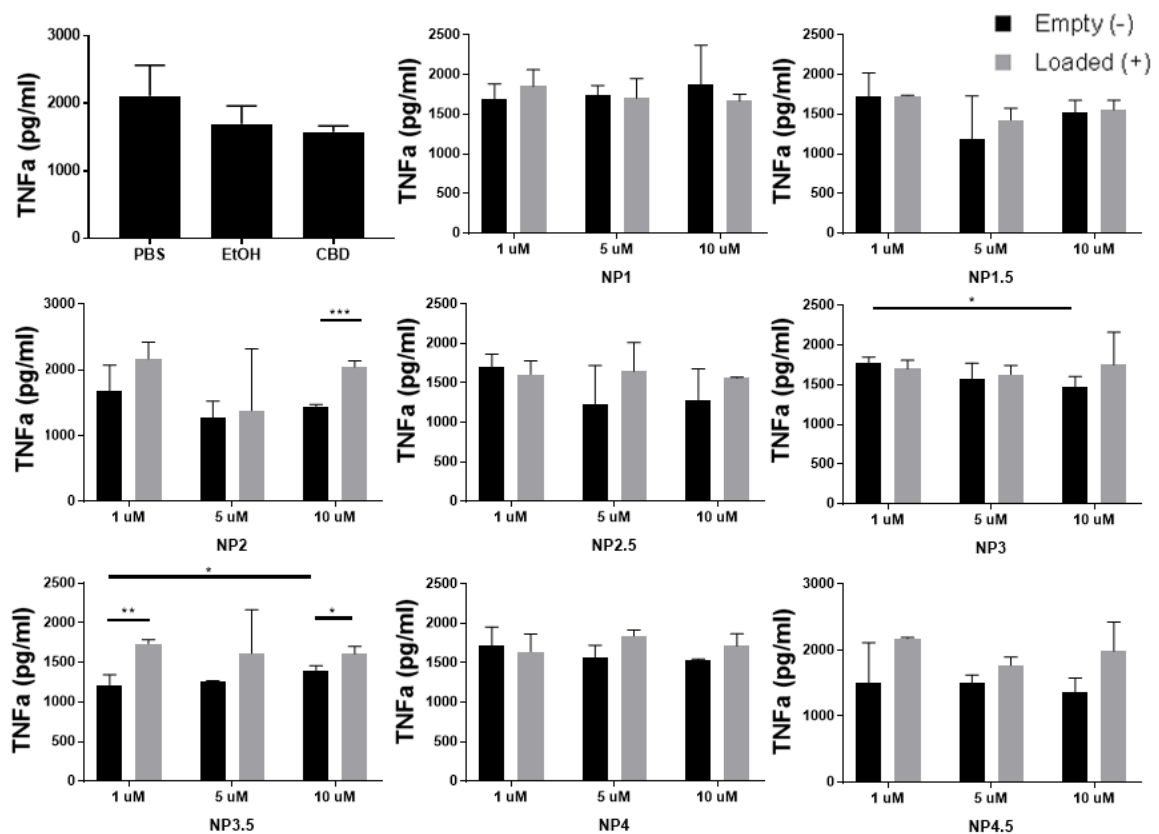

Figure 3.11: **TNFα concentration measurements after 24h incubation of NPs diluted in PBS (n=3)**. The upper left graph show the TNFα concentration of the control groups with 10 μM ethanol and CBD. The other graphs compare the empty (black) and loaded (grey) NPs added in three different concentrations. Error bars are SDs. Statistics was calculated with the two way student t-test. Statistically significant of P<0.05, P<0.01 and 0.001 are annotated with *, ** and *** respectively.

The IL-12 production of the various treatments is summarized in Figure 3.11. The first thing we can see is that the CBD singularly already decreases the IL-12 production (P<0.05). The ethanol does not significantly decrease the IL-12 therefore it is safe to assume that the CBD single-handedly is the cause of the decrease. Although there is for most cases not a considerable difference between loaded and empty particles, most samples already perform better than the PBS control. Besides NP1- (1 and 10 μM) every sample significantly decreases the IL-12 production (P<0.05). NP3.5 again stands out and shows a clear difference between empty and loaded particles (P<0.01) for all the concentrations. Most samples are however scattered around and show great variability which makes comparing them difficult.
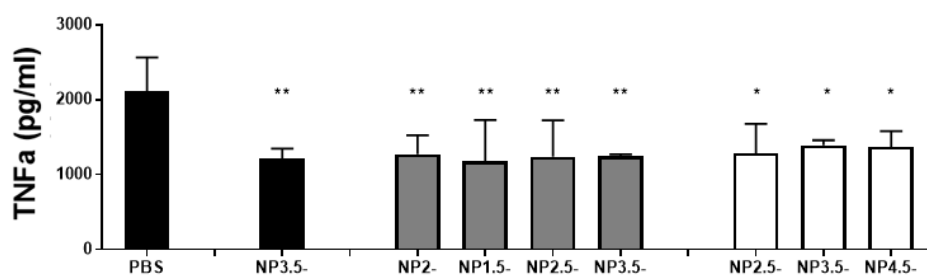
Figure 3.12: **Significant decreased TNFα production in NPs treated samples (n=3).** Each samples was compared to the PBS control group and the significantly different treatments are summarized in this figure. Black bars indicate the 1 μM added conditions, grey bars indicate 5 μM and white bars indicate the 10 μM. Error bars are SDs. Statistics was calculated with the two way student t-test. Statistically significant of P<0.05 and P<0.01 are annotated with * and ** respectively.
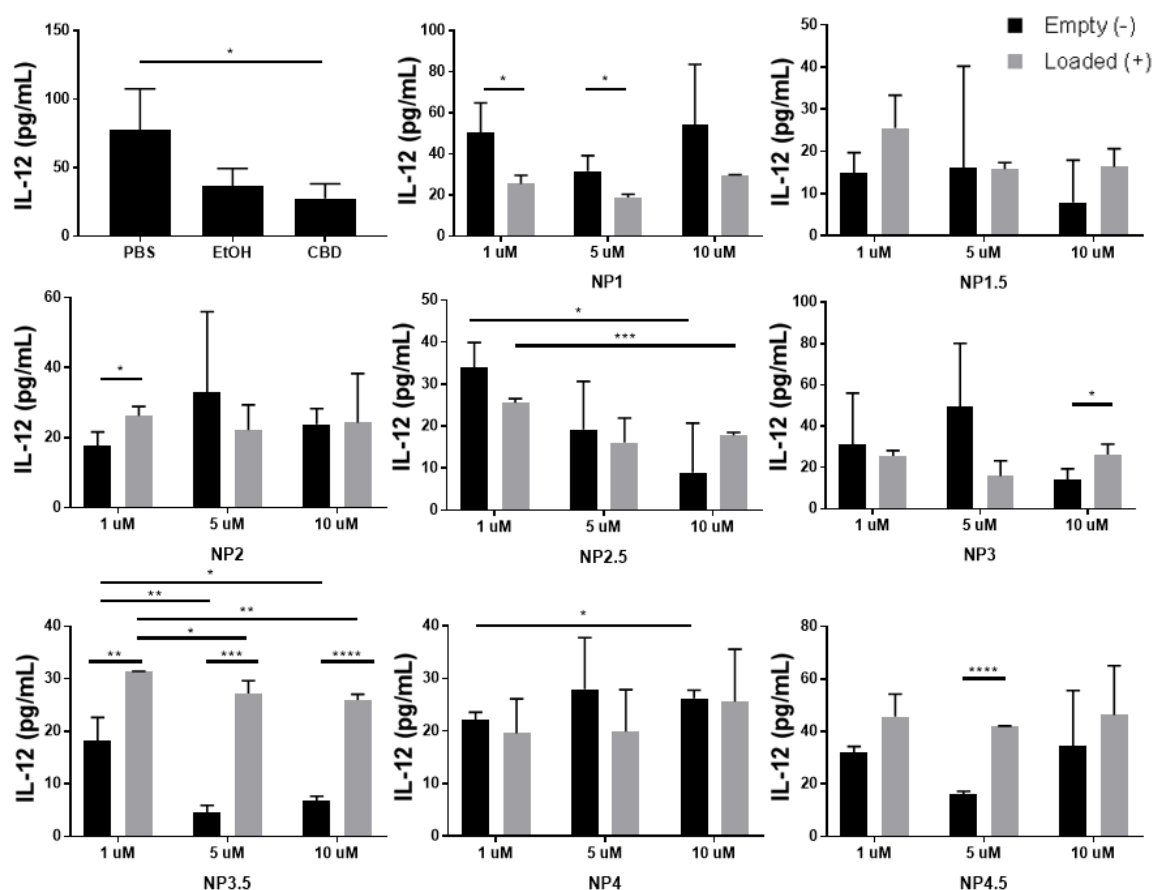

Figure 3.13: **IL-12 concentration measurements after 24h incubation of NPs diluted in PBS (n=3).** The upper left graph show the IL-12 concentration of the control groups with 10 μM ethanol and CBD. The other graphs compare the empty (black) and loaded (grey) NPs added in three different concentrations. Error bars are SDs. Statistics was calculated with the two way student t-test. Statistically significant of P<0.05, P<0.01, P<0.001 and P<0.0001 are annotated with *, **, *** and **** respectively.

4

Discussion

In this research we wanted to prepare different types of HDL based NPs and test their targeted delivery of cannabinoids to pro-inflammatory macrophages, specifically in AS.

4.1. Nanoparticle synthesis and characterization

To gain the advantages of the nano-scale it was important for the particles to remain in the range of 10 to 100 nm. For the top down synthesized particles this was indeed the case. The majority of the samples remained stable and in the targeted range. A previous study which also analyzed HDL based NPs with similar formulations found smaller DLS measured sizes for their samples [51]. The measured diameters were in the range of 10 to 40 nms for the samples without cholesterol or polymers. Our results however suggest sizes of 40 nms and above which could be the result of the method used. Longer sonication time is linked to decreasing particle sizes and in our research the sonication time did vary among the samples [52].

Generally speaking, sonication was stopped when the mixture became clear, which is a subjective decision based method. Some samples did require a longer time to become transparent, in particular samples with CBD and cholesterol took longer. These samples particularly are bigger than the NPs without drug or cholesterol. Combining the fact that the sonication time was longer and the samples were significantly bigger, except NP4.5, it is possible that these samples started of bigger and are more difficult to shrink. Hence this could explain why these samples are unstable after 30 days, specifically their observed drop in size. An optical absorbance measurement could have been used as an objective alternative. However some samples have a higher concentration of unprocessed compounds (e.g. loose phospholipids). Sonicating all the samples for an equal amount of time sounds like a better approach however sonicating samples for longer could damage the molecules and sonicating other samples for a shorter period would create micro-particles.

Adding triglyceride or using longer tailed phospholipids (POPC and PHPC) did not influence the size significantly, which was also observed in Tang et al. [51]. However they do influence the observed TEM images. Looking at the morphology it can be seen that the triglyceride does create a more spherical shape, which is also observed in the same study [51]. Analyzing a naive HDL protein triglyceride is a well known component, besides the phospholipids and ApoA1 protein [53]. Naive HDLs are also spherical shape which could be the result of the triglyceride in the core.

POPC is a saturated phospholipid with a longer hydrophobic tail compared to DMPC. Its hydrophobicity is also slightly higher than DMPC which could improve the synthesis but decrease affinity with cholesterol [54] [55]. The synthesis improvement can be demonstrated in higher phospholipid yields which is also seen in Figure 3.5. Based on the research it is however unclear what implications the decreased cholesterol affinity has if even at all. What is interesting to note that the POPC and PHPC based NPs had difficulty in the dry environments of the TEM. Since the POPC and PHPC phospholipids are more fluidity they do loose their shape and strength in the dry conditions. In the Tang et al, article this also seemed to appear in the supporting figures [51]. Other methods like scanning electron microscopy or atomic force microscopy in fluid cells could be used as well to determine the morphology of the NPs. The measurements between the DLS and TEM for the other samples are consistent it is

therefore safe to assume that the samples that were not well measurable with TEM have the diameter in the range of the DLS measurements.

In this research we briefly touched upon the use of polymers. Specifically PLA and PLGA, which are used in new stenting designs, due to their biocompatibility and degradation rates. The polymers could potentially, improve the stability and create a more gradual drug release profile [44]. In our results the incorporation of polymers, using the bottom up approach, did create spherical NPs, even without the triglyceride. The NPs also became relatively bigger compared to the top down approach. A higher polymer to phospholipid ratio increased the size considerably. The PGNP2 and PLNP2 both were out of the range required, which was most likely the result of the higher concentration of polymers added. These formulations were also performed in the Tang et al, article however the measured sizes did not agree with ours [51]. Firstly, our samples remained below 120 nm and most even below 100 nm which was one of our requirements. Looking further into their methods two parameters seem to be different, namely the injection rates and the ApoA1 concentration. The higher speed and higher concentration ApoA1 used in our method could explain the shrunken size compared to their results. Because we require a maximum size of 100 nms our used method is more favorable. The polymer incorporated samples were better measurable with TEM and were in agreement with the DLS measurements (Figure 3.2). These samples were not further studied since the CBD loading measurements using LC-MS because a proper method still had to be developed to take into account the polymers in the formulation. Although these particles were not further developed they could have potential for future research. A disadvantage to consider however is the fact that a partial volume of the NPs cores is taken up by the polymers and subsequently less volume is available for drug incorporation.

Because of the limited equipment and time only a single sample was analyzed for its CBD content. It is likely that there is a variance between the particles, just like phospholipid yield. Nonetheless since the sample preparation and materials are similar we would assume there would not be a drastic decrease in CBD yield. Until the other samples are measured it is not possible to conclude this, only speculate.

When looking at the ζ-potential measurements in 10 μM HEPES (Figure 3.3) it can be said that the CBD and cholesterol do not influence the ζ-potential considerably. Therefore it can be speculated that both the CBD and the cholesterol are mainly located in the core of the NPs. However, not all samples could be measured because of the limited material available. The NP3.5 and NP4.5 samples were not measured and therefore the interaction of cholesterol and POPC and PHPC could not be further analyzed. Moreover it could be possible that the affinity difference between DMPC and POPC with cholesterol influences the ζ-potential. Only the NP1 shows a significant difference between the unloaded, loaded and cholesterol incorporated samples. The empty NP1 sample interestingly touches the -30 mV barrier which was desired. Strikingly this is only the case in 10 μM HEPES, the same sample in 5% glucose shows a great drop in ζ-potential. The other samples showed insignificant changes. The ζ-potential was expected to increase in 5% glucose compared to the 10 μM HEPES. Since fewer ions are present almost all would accumulate around the NPs surfaces and a big difference between the cloud and the medium should be observed [43]. The 5% glucose measurements were performed 2 weeks after the 10 μM HEPES measurements, which could be sufficient time for the samples to become more unstable even if the DLS measurements do not show this. Moreover a small volume of the samples was diluted in the 5% glucose and 10 μM HEPES which could contain too few NPs for proper measurements. It would be advisable to dilute the entire sample in the measurement media. This could be done using a centrifugal filtration, while adding either glucose or HEPES. If this also does not create a sufficient surface potential a different medium for *in vivo* testing should be considered. Unfortunately the Zeta Nanosizer was unable to perform measurements in the PBS medium (in which the samples were stored) since it would damage the instrument (ionic strength = 2.1μM). We could assume that these particles remain stable in this medium based on the DLS measurements, but there is no additional argument to back this up.

The protein assay used to determine the ApoA1 yield was ineffective (Figure 3.4). The compounds or structures in the samples seem to interference with the BCA kit. Upon reading the compatibility chart of the BCA kit it becomes clear that PBS could interfere with the assay. Limited information on the PBS concentration limit and the type of interference was available. The samples with triglyceride generally seemed to interfere more with the assay than the NPs without (NP2, NP2.5, NP4 and NP4.5). This is not clearly stated in the compatibility chart. The ApoA1 stock measurements did however agree with the expected results, regardless of PBS. It is thus safe to assume that the ApoA1 protein is compatible with

the BCA method. The expected ApoA1 stock concentration was obtained by using another method. This method is however not compatible with the phospholipids in our samples. An additional DC based protein assay was performed however interference was again observed (specifically NP2 and NP4) (Appendix C). HDL samples are not commonly measured for their protein yield in the literature which makes it difficult to compare. Another technique that could be used is LC-MS which could be done in the future. In collaboration with the GMZ at the AMC this could be achieved, however due to the high demand of their equipment this could not be done within the time.

Our phospholipid assay results demonstrate that the top down approach has an acceptable yield (Figure 3.5). Although the NP1 samples had a relatively low yield it was still above 50%. This only further increased when adding triglyceride (NP2) or cholesterol (NP1.5). The samples containing POPC and PHPC all had greater yields compared to the DMPC, MHPC samples. The long phospholipid chains and the higher hydrophobicity possibly increased the phospholipid yield [55]. The CBD did not seem to interfere with the method nor did it influence the yield significantly. Because the NPs were added to the cells according to their phospholipid yield it is important to analyze if the *in vitro* results were not influenced by this. The phospholipid yield was compared to the NO,TNFα and IL-12 response and no distinct trend was observed (not presented in the thesis). It is therefore plausible that the *in vitro* results were not the result of the phospholipid yield but it is not possible to exclude the thought entirely. Using a different method to normalize the *in vitro* conditions could be used (e.g. CBD yield or NPs count).

The entrapment efficiency of CBD was relatively low (around 20%) but not uncommon in the used method [56]. However NPs have the capacity to reach entrapment efficiency percentages of almost 100% but are mostly around 70 to 80% [52]. Our results are clearly still very low and there are several methods to improve this. One method, that does however not suit our objective, is increasing the particle sizes. It is also possible to concentrate the mixture in the method part (by adding less PBS), which would allow for an increased entrapment of the drug molecules. Several cycles of freezing and thawing increase the drug penetration into the NPs. Nonetheless these methods are considered passive, and are only able to improve the efficiency to a certain extend. Active loading techniques exists which could have a stronger impact. Several of these techniques are reviewed in Gubernator et al, which covers methods such as generated proton or pH gradients [56]. There are thus several techniques that can be used to improve the entrapment.

4.2. *In vitro*

In agreement with the literature, the cannabinoid receptors are more abundantly present in the pro-inflammatory macrophages (LPS + IFNγ + Acetyl-LDL) compared to the other types of macrophages (Figure 3.7) [57]. Additionally the shape and morphology in the different conditions are similar to published work [58]. Moreover this confirmation aids in our hypothesis that the cannabinoid receptors, specifically CB_2, is a specific enough target. Interestingly CB_1 is also overly expressed in the pro-inflammatory macrophages. It is expected that the CB_2 is more abundantly present on these macrophages, but with the staining method used it is not possible to compare them both. CB_1 requires different staining antibodies with different dilutions. It is noteworthy that the literature states that CB_1 is also mostly present on neuron cells [16]. In our research we did not analyze neuron cells on cannabinoid receptor expression but it would be interesting for a future study. CBD, specifically, has similar affinities towards CB_1 and CB_2 receptors which could influence the NPs uptake into the plaque. On the contrary, the permeability of AS plaque is much greater than that of the blood brain barrier, which could be in our advantage.

When looking at the plaque sections there seemed to be colocalization between the macrophages and the cannabinoid receptors (Figure 3.8). This does agree with the literature and strengthens our hypothesis. As an additional supplementary study the effect of the NPs on the cannabinoid receptor expression in single macrophages could be studied. It would be interesting to see if the receptor expression decreases, which is what would be expected when the inflammation, partially, is relieved. If *in vivo* research will be done, it would be valuable to locate the nanoparticles in different tissues. Methods like super-resolution microscopy allow for a reliable location detection. Fluorescent labeling of the NPs can be done similar to the research done in Tang et al. [51].

The *in vitro* results create a lot of material to discuss. First the NO concentration does not seem to be effected by the CBD neither by the ethanol in the admitted concentrations of 10 μM. The NO

concentration also does not increase in any NPs treatment conditions up to 10 μM, suggesting that limited cell arrest and apoptosis occurred (NO on cell proliferation). In a handful of samples the NO concentration dropped significantly. Nonetheless the measured concentrations are not low enough to shift the cell signaling [47].

The difference between the 1, 5 and 10 μM NPs treatments does seldom correlate to NO concentration. We can thus assume one of two things, either the concentration range is too low to critically effect the cell signaling dynamics, or the minimum concentration is already high enough to induce the maximum effect on these dynamics. The prior one is most likely, since differences can be observed, between and among the samples. Nonetheless a 3-(4,5-Dimethylthiazol-2-yl) -2,5- diphenyltetrazoliumbromidefor (MTT) test would be advised perform in the future. the MTT test would qualitatively measure the cell viability using a range of different concentrations, for example from 0 up to 50 μM.

When comparing the different formulations with each other the effects of triglyceride, phospholipids, CBD and cholesterol can be analyzed. Firstly, the addition of triglyceride (comparing NP1 to NP2 and NP3 to NP4) does not considerably shift the NO concentration. NP4 does seem to have lower NO concentrations, which we will discuss shortly. The different phospholipids (comparing NP1 and NP2 to NP3 and NP4) also do not give an indication of change. This is the case for samples with and without cholesterol. Overall, the loaded samples exhibit lower NO concentrations compared to their empty counterparts, except for NP4. The reason for the NP4 samples (containing POPC, PHPC and triglyceride) behaving differently is still unclear. Because CBD is an inflammation reliever it could result in decreased cellular stress, and also NO concentration. The samples containing cholesterol in general do not differ considerably from their non-cholesterol embedded counterparts. Because each component, individually, is in relatively low concentration present in the medium their effects written in the literature are not comparable.

The range of concentrations used did not particularly influence the results greatly for either cytokines. Only in the cases of NP2.5 and NP3.5, both loaded and empty, does there appear a significant drop in TNFα and IL-12 production with higher NP concentration. For the other samples we could suggest that the treatment concentration range was either too low or already high enough for an effect to occur. In a test experiment, presented in Appendix E, a lower concentration was used under slightly different conditions. A 0.1μM concentration shows no significant difference with the 1 and 5 μM treatments. Although the conditions are different in that experiment we can still speculate that the concentrations used in the body of the thesis could be too low to influence the results. The triglyceride, phospholipids and cholesterol changes in the formulation do appear to shift some of the results. Unfortunately no clear trends could be extracted from the different formulations due to fluctuations and inconsistencies.

The TNFα and IL-12 results also provide several parts to discuss. As expected none of the treatments considerably exceeded the control group's cytokine production. The anti-inflammatory effect of CBD, singularly, can not be seen on the TNFα graphs but do appear in IL-12 (Figures 3.11 and 3.13). Because the CBD single-handedly did not change the TNFα production it is to no surprise that the loaded samples did not perform better than their unloaded counterparts. But interestingly, almost all the samples that showed a significant decrease in TNFα production, in comparison to PBS, were unloaded (Figure 3.12). As for the IL-12 cytokine production, the results are more scattered around. With some loaded samples performing better than the unloaded samples and vice versa.

The results still seem to be fluctuating, which could indicate that the *in vitro* model still requires fine tuning. It also appeared to be difficult to find another cause for the fluctuation and little is comparable with published research. From what we do know we can however speculate about some of the observed data. The first thing to note is that the CBD content in the particles did appear to be low (around 20%), which could explain why the loaded samples did not perform better than the unloaded samples for IL-12 production. It does however not explain why they perform worse. Sadly, the drug content of the cholesterol embedded NPs is not yet known, so we cannot compare them yet. Also, we do not know the drug release profiles yet of the different samples. In theory the less stable NPs would have a quicker release of a large portion of their drug compared to the more stable ones. We could observe in the DLS measurements (Figure 3.1) that the cholesterol embedded samples, specifically NP2.5 and NP3.5, were more unstable than the others. Yet again the unloaded NP2.5 and NP3.5 samples performed better, meaning the quick and fast drug release did not correlate to the performance.

What we do know is that HDL is involved in cholesterol efflux, but in these conditions no lipids were

added, meaning that the HDL could influence other complementary pathways. It would be interesting to investigate what HDL does more in pro-inflammatory macrophages.

4.3. Future work

Based upon the research performed and the literature we present a couple of recommendations for the future. Firstly, the cholesterol incorporation should be stabilized, maybe starting with a lower concentration of cholesterol. Not only would we expect a greater stability but also smaller NP sizes. For the polymer incorporation, CBD should be added to the formulation to see the effect on size and determine the loading yield. Also based upon our measured drug loading yield in the conventional particles, the formulation could be altered.

Thereafter a drug release profile is essential, which can be done using different methods. The first method would be LC-MS based, which includes several measurements over time. With filtering techniques a distinction can be made between the incorporated and circulating drug. It is important that the filtering technique does not damage the NPs. Another technique relies on absorbance measurements of leaking CBD. The samples are presented, in a permeable bag or sheet, to a larger medium volume. The permeable bag only allows for structures below a certain size to diffuse out into the larger medium. Samples taken from the larger volume are measured and the absorbance can be converted into a concentration. The hydrophobicity of the drug should be considered during this measurements, since they will not diffuse freely in a hydrophilic medium.

In the case of CB_1 receptors, their presence on neurons could effect *in vivo* delivery. We therefore propose testing different cannabinoid compounds with greater affinity toward CB_2 for example JWH-133. This cannabinoid has a 20X affinity with CB_2 compared to CB_1 and shares great chemical similarity with CBD [59]. Because we compared different particles in this research, it would be of added value to research different drug types as well.

To complete the *in vitro* tests various parameters have to be fine-tuned. These include incubation time, NP concentration and protein and mRNA expression. Other pro- and anti-inflammatory cytokines could also be measured to get an overall picture. Shifts in mRNA expression could be further indication of the NPs treatment effects. Also, as mentioned previously, a MTT test is crucial before further *in vitro* tests will be performed, since a qualitative cell viability could support or debunk the NPs treatment effect.

We already know that the NPs accumulate largely in the AS plaque, therefore it would be interesting as a final *in vitro* experiment to determine the NPs binding specificity in a medium with different cell types. Briefly, adding an equal amount of endothelial cells, SMCs and macrophages to a well, as well as three different wells containing one single cell type, and incubate them with fluorescent labeled NPs. After treatment these can be fixed and stained using cell specific markers. With the help of super-resolution microscopy the specificity of the NPs can be determined. This would be a good basis for a future *in vivo* experiment in which a similar, but systematic, treatment is added and various cells will be analyzed. Similar to Tang et al. an *in vivo* fluorescent labelled NP treatment experiment can be performed [51].

5

Conclusions

It cannot be stressed enough that cardiovascular diseases take a huge toll on the western world both in numbers and costs, with atherosclerosis being the main cause of these diseases. Pro-inflammatory macrophages, specifically foam cells, are a distinct phenotype of this disease. A phenotype that we tried to use to our advantage in regressing the condition, specifically the cannabinoid receptors. We synthesized various nanoparticle delivery systems, based upon high density lipoproteins, and characterized their physical and physiochemical properties. This library of carriers was loaded with the, well documented, cannabidiol drug and incubated with pro-inflammatory macrophages. In the characterization step it can be seen that triglyceride rounded the nanoparticles. Adding cholesterol in general increased the size of the particles but destabilized them quicker. The dynamic light scattering results were in agreement with the transmission electron microscopy results. The particles had an inadaquate surface charge in both 10μM HEPES and 5% glucose but are independent from cholesterol, triglyceride or cannabidiol. In general the samples containing 1-palmitoyl-2-oleoyl-sn-glycero-3-phosphocholine (POPC) and 1-palmitoyl-2-hexadecyl-sn-glycero-3-phosphocholine (PHPC) had a greater assembly yield than the nanoparticles with 1,2-dimyristoyl-sn-glycero-3-phosphocholine (DMPC) and 1-myristoyl-2-hydroxysn-glycero-3-phospho- (1'-rac-glycerol) (MHPC). The cannabidiol yield is low, below 50%, this has to be improved for the future. Nonetheless, even with this low concentration the effects are still seen in the *in vitro* assays. Our hypothesized target (the cannabinoid receptors) showed to be abundant in pro-inflammatory foam cells and highly selective for macrophages in general. Finally, the *in vitro* results showed some unexplained differences between the treatment conditions, nonetheless the Nitric Oxide concentrations are promising as well as the IL-12 results. Still some questions remain and many experiments are yet to be performed before nanoparticles can be used as an effective treatment for atherosclerosis.

Acknowledgement

I would like to use this opportunity to express my gratitude to the people who helped me throughout my thesis. First and foremost I would like to thank my head supervisor Dr. I. Apachitei for allowing me to work in this topic, for both guiding me throughout the steps and for giving me constructive feedback. I would also like to thank my second supervisor E. Kluza for providing me with a position in her group at AMC on the experimental vascular biology department and for a project topic in my interest field. I would like to take the opportunity to thank Vivian de Waard from the AMC of a different research group, who encouraged me in my work and with whom I was able to discuss new ideas for the project. Finally I would like to give a special gratitude to my direct supervisor Mr. T. J. Beldman who both helped me start up my research and encouraged me to find new perspectives.

Appendix

5.1. Appendix A

The Herringbone mixer principle

A Herringbone mixer consists of a rectangular or circular channels with herringbone grooves embedded in its surface at alternating 45 degree angles (Figure 5.1). The width and height of the channels are usually in the range of 100 to 200 μm while the grooves usually have a width around 35 μm [60]. The entire length of the Herringbone mixer is roughly 600 μm and consists of two micro-channels that meet before the herringbone grooves are embedded. Hereafter the fluids mix under controlled conditions. Because of the dimensions the viscosity of the fluids dominates the process [61]. The grooves themselves allow for vortices to develop, while the shifting orientation of the angles disrupts the flow. These two forces allow for proper and chaotic distribution of molecules on the micro-scale while using a continuous flow [60]. Many models and designs exists and in our experiment we used the one presented in Figure 5.2.
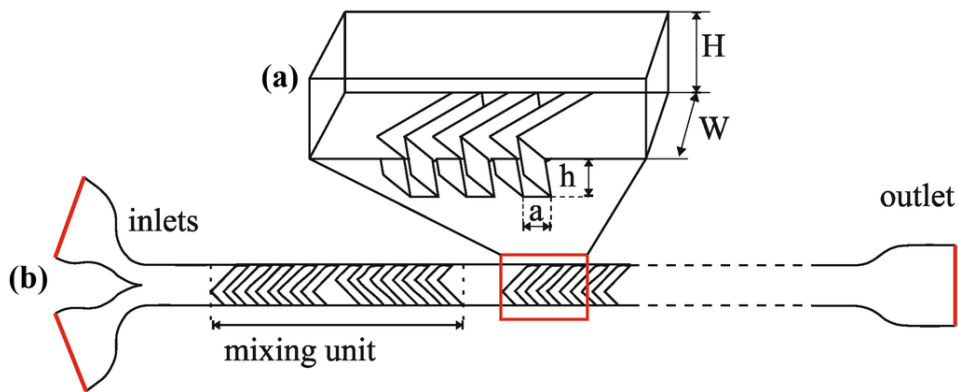
Figure 5.1: **General model of a Herringbone mixer with its grooves [60].** (a) One unit of herringbone grooves is illustrated in three dimensions. The grooves are at an angle of 45 degrees with the surface. The H and W represent the height and width of the entire channel and are greater than the height and width (h and a) of the groove. (b) The micro-channels inlets meet halfway before the mixture units. These units are only present in the body of the herringbone and alternate to disrupt the flow. At the outlet the grooves are gone and the mixture can be caught.
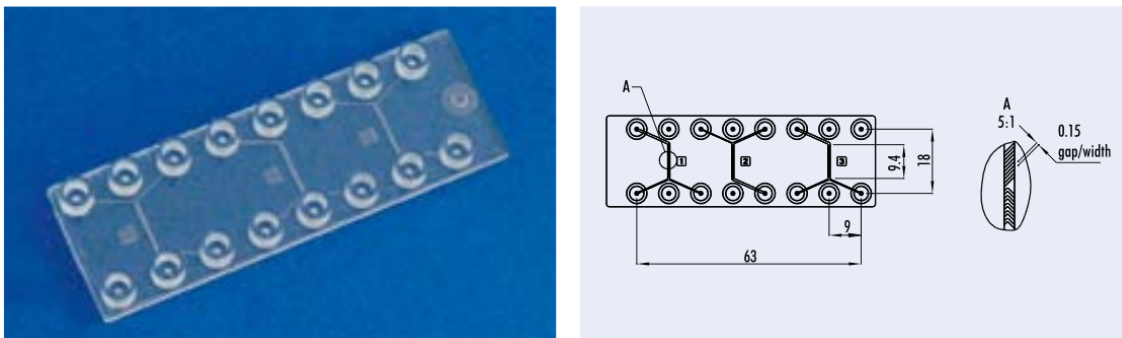

Figure 5.2: **Herringbone design drawings.** The specific herringbone mixer used in this experiment is presented to the left. On the right side the industrial drawing of the company is shown with the dimensions and grooves [62].
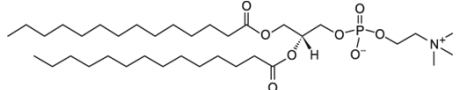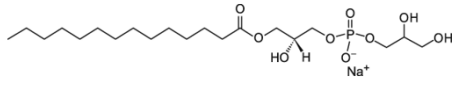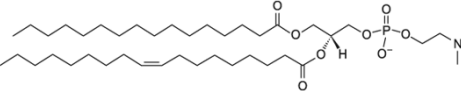
5.2. Appendix B
Lipid and polymer details

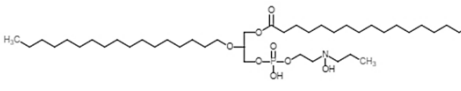| Abbreviation	Chemical structure	Chemical formula	Molar mass
DMPC	1,2-dimyristoyl-sn-glycero-3-phosphocholine	$C_{36}H_{72}NO_8P$	677.945
MHPC	1-myristoyl-2-hydroxy-sn-glycero-3-phospho-(1'-rac-glycerol)	$C_{20}H_{40}O_9PNa$	478.490
POPC	1-palmitoyl-2-oleoyl-sn-glycero-3-phosphocholine	$C_{42}H_{82}NO_8P$	760.09
PHPC	1-palmitoyl-2-hexadecyl-sn-glycero-3-phosphocholine	$C_{40}H_{84}NO_8P$	495.64

Figure 5.3: **Chemical properties of the phospholipids used in this research.** The abbreviations used in the body of the thesis, followed by the chemical structure and full name. In the final two columns the chemical formula and the molar mass (g mol^{-1}) are presented.
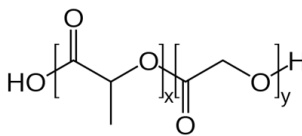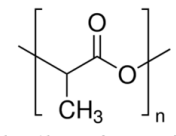
	Chemical structure
PLGA	Poly(lactic-co-glycolic acid)
PLA	Poly(lactic acid)

Figure 5.4: **Chemical properties of the polymers used in this research.** The abbreviations used in the body of the thesis, followed by the chemical structure and full name.
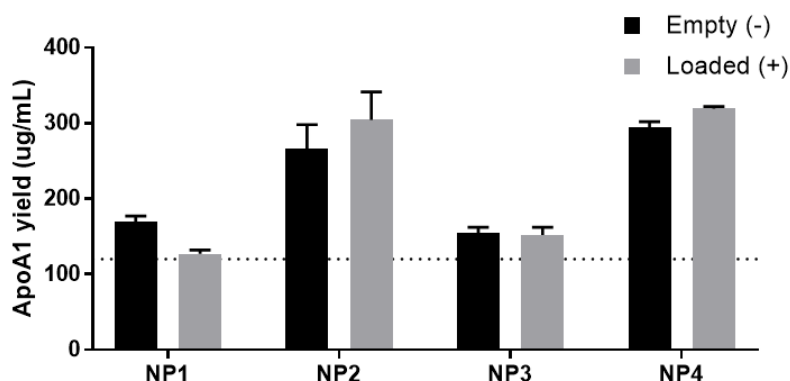
5.3. Appendix C
DC protein assay

Figure 5.5: **ApoA1 protein concentration measured using the DC protein kit (n=3)**. The dotted line represents the ApoA1 input for the empty (-) and loaded (+) NPs. Again interference can be observed from the particles.
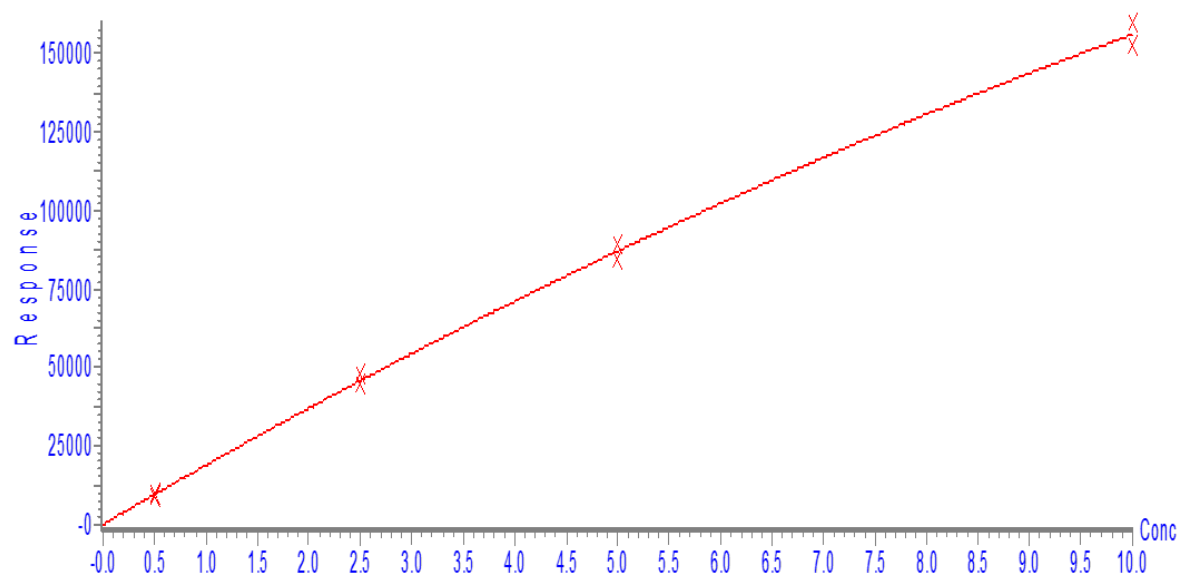
5.4. Appendix D
CBD calibration curve

Figure 5.6: **The calibration curve provided by the GMZ presenting the concentration (μM) against the response signal of the LC-MS (n=2)**. The red X's indicate the measurements done using the LC-MS. The 10μM CBD diluted in ethanol shows a linear regression curve (red dotted line).

5.5. Appendix E
Additional *in vitro* results

The cells were derived from wild type C57BL/6 mice and cultured in RPMI-1640 medium with 15% LCM. The overall method was similar to sections 2.4.2 but the cells were promoted, only with LPS and without IFNγ. Also the NPs were incubated for 72 hours with the cells instead of 24 hours. The NPs sample concentrations were 0.1, 1 and 5 μM. Large differences and big standard deviations were observed. Also the TNFα and IL-12 control concentrations were too low to be considered inflammatory. Nonetheless, differences could be fond between loaded and unloaded samples. No cells were treated with NPs containing cholesterol, because of limited material.
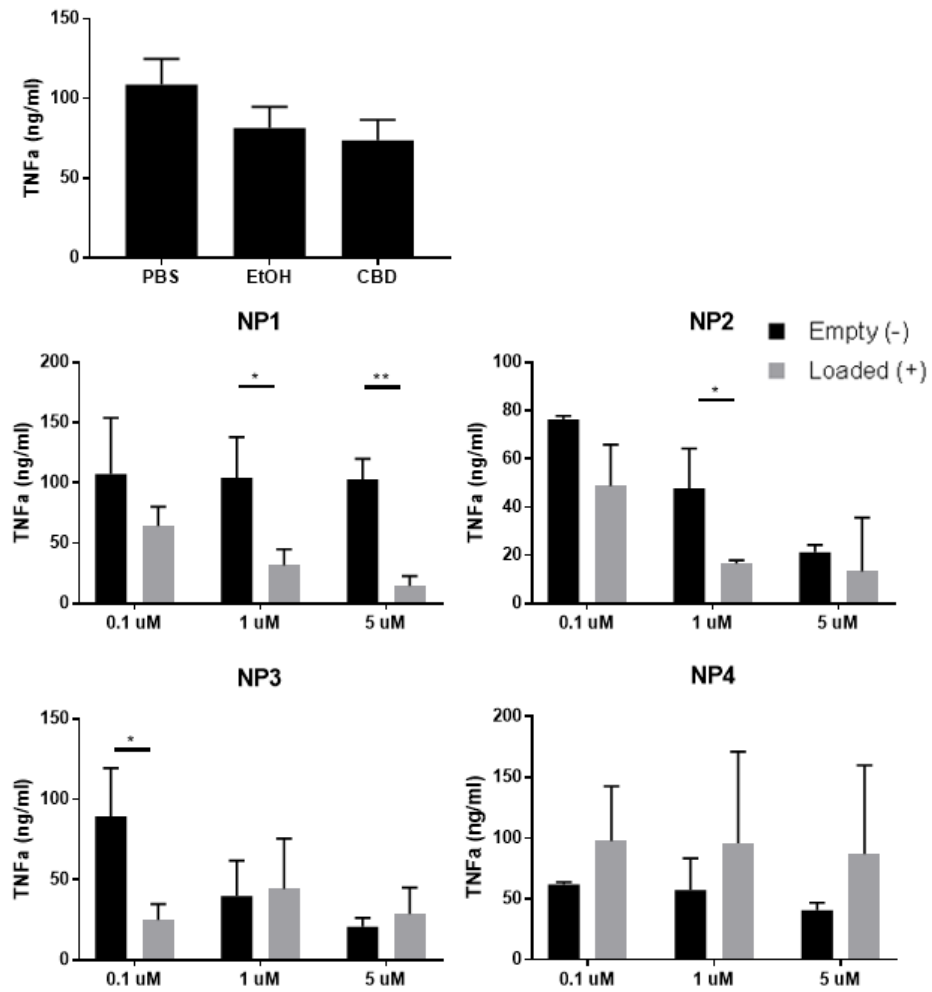
Figure 5.7: **TNFα concentration measurements after 72h incubation of NPs diluted in PBS (n=3)**. The upper left graph show the TNFα concentration of the control groups with 1 μM ethanol and CBD. The other graphs compare the empty (black) and loaded (grey) NPs added in three different concentrations.Error bars are SDs. Statistics was calculated with the two-way ANOVA test.
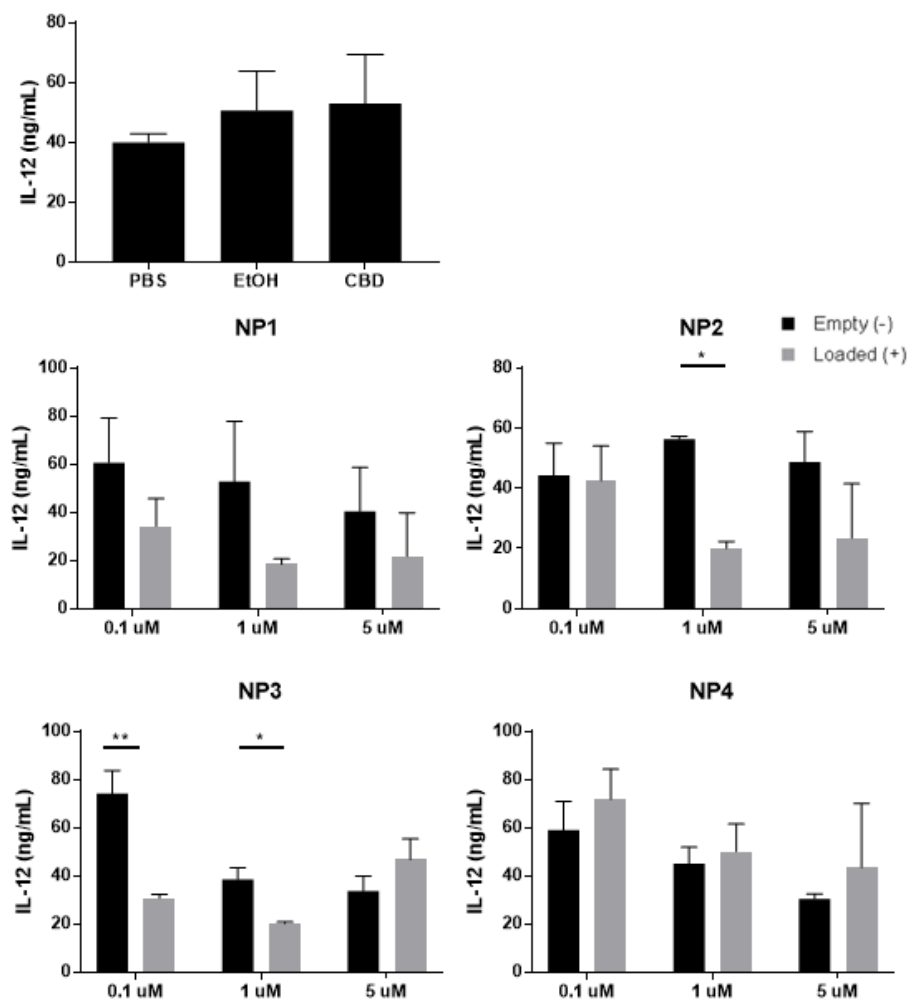
Figure 5.8: **IL-12 concentration measurements after 72h incubation of NPs diluted in PBS (n=3).** The upper left graph show the IL-12 concentration of the control groups with 1 μM ethanol and CBD. The other graphs compare the empty (black) and loaded (grey) NPs added in three different concentrations.Error bars are SDs. Statistics was calculated with the two-way ANOVA test.

References

[1] G. H. Gibbons, *Nhlbi fiscal fact book 2012,* (2012), u.S.A. National Institutes of Health consulted on 05-09-2016.

[2] D. Mozaffarian, E. Benjamin, A. Go, D. K. Arnett, M. J. Blaha, M. Cushman, S. R. Das, M. Sarah de Ferranti, J.-P. Després, H. J. Fullerton, *et al.*, *Aha statistical update,* Heart Dis. stroke **132** (2015).

[3] E. Galkina and K. Ley, *Immune and inflammatory mechanisms of atherosclerosis,* (NIH Public Access, 2009) p. 165.

[4] J. F. Bentzon, F. Otsuka, R. Virmani, and E. Falk, *Mechanisms of plaque formation and rupture,* (Am Heart Assoc, 2014) pp. 1852–1866.

[5] M. Simionescu and A. V. Sima, *Inflammation and atherosclerosis,* (Springer, 2012) Chap. Morphology of Atherosclerotic Lesions, pp. 18–37.

[6] H. Itabe, *Oxidative modification of ldl: its pathological role in atherosclerosis,* (Springer, 2009) pp. 4–11.

[7] E. N. Marieb and K. Hoehn, *Human anatomy & physiology,* (Pearson Education, 2007) Chap. 19: The Cardiovascular System: Blood Vessels, pp. 714–723, 9th ed.

[8] L. Nielsen, B. Nordestgaard, S. Stender, and K. Kjeldsen, *Aortic permeability to ldl as a predictor of aortic cholesterol accumulation in cholesterol-fed rabbits.* (Am Heart Assoc, 1992) pp. 1402–1409.

[9] A. Sima, C. Stancu, E. Constantinescu, L. Ologeanu, and M. Simionescu, *The hyperlipemic hamster-a model for testing the anti-atherogenic effect of amlodipine,* (Wiley Online Library, 2001) pp. 153–162.

[10] H. Sugi, *Current basic and pathological approaches to the function of muscle cells and tissues - from molecules to humans,* (INTECH Open Access Publisher, 2012) Chap. 11: Vascular Smooth Muscle Cells and the Comparative Pathology of Atherosclerosis, pp. 233–254.

[11] S. Rensen, P. Doevendans, and G. Van Eys, *Regulation and characteristics of vascular smooth muscle cell phenotypic diversity,* (Springer, 2007) pp. 100–108.

[12] I. Palomo, C. Toro, and M. Alarcón, *The role of platelets in the pathophysiology of atherosclerosis (review),* Mol Med Rep **1**, 179 (2008).

[13] Y.-j. Geng, T. Kodama, and G. K. Hansson, *Differential expression of scavenger receptor isoforms during monocyte-macrophage differentiation and foam cell formation.* (Am Heart Assoc, 1994) pp. 798–806.

[14] Y. Nakagawa and K. Chiba, *Role of microglial m1/m2 polarization in relapse and remission of psychiatric disorders and diseases,* (Multidisciplinary Digital Publishing Institute, 2014) pp. 1028–1048.

[15] P. Nagarkatti, R. Pandey, S. A. Rieder, V. L. Hegde, and M. Nagarkatti, *Cannabinoids as novel anti-inflammatory drugs,* (Future Science, 2009) pp. 1333–1349.

[16] F. Astruc-Diaz, *Cannabinoids delivery systems based on supramolecular inclusion complexes and polymeric nanocapsules for treatment of neuropathic pain*, Ph.D. thesis, Université Claude Bernard-Lyon I (2012).

[17] T. Seimon and I. Tabas, *Mechanisms and consequences of macrophage apoptosis in atherosclerosis,* (ASBMB, 2009) pp. 382–387.

[18] D. Shier, J. Butler, and R. Lewis, *Hole's human anatomy,* (McGraw-Hill, 1996) Chap. 14: Blood, pp. 545–550.

[19] R. R. Razi, S. S. Brar, M. B. Jorgensen, I. Finn, and D. Zisook, *The effect of primary prevention statin therapy on mortality in persons with aortic atherosclerosis,* (Am Heart Assoc, 2016) pp. A15204–15204.

[20] L. Räber, M. Taniwaki, S. Zaugg, H. Kelbæk, M. Roffi, L. Holmvang, S. Noble, G. Pedrazzini, A. Moschovitis, T. F. Lüscher, *et al.*, *Effect of high-intensity statin therapy on atherosclerosis in non-infarct-related coronary arteries (ibis-4): a serial intravascular ultrasonography study,* (Eur Soc Cardiology, 2015) pp. 490–500.

[21] H. Okuyama, P. H. Langsjoen, T. Hamazaki, Y. Ogushi, R. Hama, T. Kobayashi, and H. Uchino, *Statins stimulate atherosclerosis and heart failure: pharmacological mechanisms,* (Taylor & Francis, 2015) pp. 189–199.

[22] S. Dagli, *What is angioplasty and stenting,* (2008), mayo Clinic consulted on 07-11-2016.

[23] M. M. Timmins, Meyer, *Effects of stent design and atherosclerotic plaque composition on arterial wall biomechanics.* Journal of Endovascular Therapy **6**, 643 (2008).

[24] J. Robinson, *Drugs to treat atherosclerosis,* (2015), webMD Medica consulted on 07-11-2016.

[25] T. E. of Encyclopædia Britannica, *Atherosclerosis pathology,* (2007), image.

[26] L.-s. Jiang, J. Pu, Z.-h. Han, L.-h. Hu, and B. He, *Role of activated endocannabinoid system in regulation of cellular cholesterol metabolism in macrophages,* (The Oxford University Press, 2009) pp. 805–813.

[27] L. Jean-Gilles, M. Braitch, M. L. Latif, J. Aram, A. J. Fahey, L. J. Edwards, R. A. Robins, R. Tanasescu, P. J. Tighe, B. Gran, *et al.*, *Effects of pro-inflammatory cytokines on cannabinoid cb1 and cb2 receptors in immune cells,* (Wiley Online Library, 2015) pp. 63–74.

[28] V. Chiurchiu, *Review, endocannabinoids and immunity,* (Mary Ann Liebert, Inc., 2016) pp. 59–66.

[29] N.N., *Agonist vs. antagonist,* (2016), new Health Guide.

[30] L. Yvan-Charvet, N. Wang, and A. R. Tall, *Role of hdl, abca1, and abcg1 transporters in cholesterol efflux and immune responses,* (Am Heart Assoc, 2010) pp. 139–143.

[31] D. K. Spady, *Reverse cholesterol transport and atherosclerosis regression,* (1999).

[32] J. F. Oram and R. M. Lawn, *Abca1: the gatekeeper for eliminating excess tissue cholesterol,* (ASBMB, 2001) pp. 1173–1179.

[33] A. Javaheri, D. M. Kolansky, and M. Cuchel, *Reconstituted high-density lipoprotein therapies,* (2014).

[34] T. Skajaa, Y. Zhao, D. J. van den Heuvel, H. C. Gerritsen, D. P. Cormode, R. Koole, M. M. van Schooneveld, J. A. Post, E. A. Fisher, Z. A. Fayad, *et al.*, *Quantum dot and cy5. 5 labeled nanoparticles to investigate lipoprotein biointeractions via forster resonance energy transfer,* (ACS Publications, 2010) pp. 5131–5138.

[35] P. G. Frank and Y. L. Marcel, *Apolipoprotein ai: structure–function relationships,* (ASBMB, 2000) pp. 853–872.

[36] J. B. Simonsen, *Evaluation of reconstituted high-density lipoprotein (rhdl) as a drug delivery platform–a detailed survey of rhdl particles ranging from biophysical properties to clinical implications,* (Elsevier, 2016) pp. 2161–2179.

[37] R. Duivenvoorden, J. Tang, D. P. Cormode, A. J. Mieszawska, D. Izquierdo-Garcia, C. Ozcan, M. J. Otten, N. Zaidi, M. E. Lobatto, S. M. Van Rijs, *et al.*, *A statin-loaded reconstituted high-density lipoprotein nanoparticle inhibits atherosclerotic plaque inflammation,* (NIH Public Access, 2014) p. 3065.

[38] Y. Zhao, I. van Rooy, S. Hak, F. Fay, J. Tang, C. d. L. Davies, M. Skobe, E. A. Fisher, A. Radu, Z. A. Fayad, *et al.*, *Near-infrared fluorescence energy transfer imaging of nanoparticle accumulation and dissociation kinetics in tumor-bearing mice,* (ACS Publications, 2013) pp. 10362–10370.

[39] Y. Zhao, F. Fay, S. Hak, J. M. Perez-Aguilar, B. L. Sanchez-Gaytan, B. Goode, R. Duivenvoorden, C. de Lange Davies, A. Bjørkøy, H. Weinstein, *et al.*, *Augmenting drug-carrier compatibility improves tumour nanotherapy efficacy,* Nature communications **7** (2016).

[40] T. J. Beldman, M. L. Senders, A. Alaarg, C. Perez-Medina, J. Tang, Y. Zhao, F. Fay, J. Deichmöller, B. Born, E. Desclos, *et al.*, *Hyaluronan nanoparticles selectively target plaque-associated macrophages and improve plaque stability in atherosclerosis,* ACS nano (2017).

[41] S. Mukherjee, S. Ray, and R. Thakur, *Solid lipid nanoparticles: a modern formulation approach in drug delivery system,* (Medknow Publications, 2009) p. 349.

[42] I. V. Zhigaltsev, N. Belliveau, I. Hafez, A. K. Leung, J. Huft, C. Hansen, and P. R. Cullis, *Bottom-up design and synthesis of limit size lipid nanoparticle systems with aqueous and triglyceride cores using millisecond microfluidic mixing,* (ACS Publications, 2012) pp. 3633–3640.

[43] N.N., *Zeta potential theory and measurements on the nicomp,* (2015), particle Sizing Systems consulted on 05-01-2017.

[44] X. Tao, S. Jin, D. Wu, K. Ling, L. Yuan, P. Lin, Y. Xie, and X. Yang, *Effects of particle hydrophobicity, surface charge, media ph value and complexation with human serum albumin on drug release behavior of mitoxantrone-loaded pullulan nanoparticles,* (Multidisciplinary Digital Publishing Institute, 2015) p. 2.

[45] B. Necula, I. Apachitei, L. Fratila-Apachitei, C. Teodosiu, and J. Duszczyk, *Stability of nano-/microsized particles in deionized water and electroless nickel solutions,* (Elsevier, 2007) pp. 514–522.

[46] L. Zhang, J. M. Chan, F. X. Gu, J.-W. Rhee, A. Z. Wang, A. F. Radovic-Moreno, F. Alexis, R. Langer, and O. C. Farokhzad, *Self-assembled lipid- polymer hybrid nanoparticles: a robust drug delivery platform,* (ACS Publications, 2008) pp. 1696–1702.

[47] C. Napoli, G. Paolisso, A. Casamassimi, M. Al-Omran, M. Barbieri, L. Sommese, T. Infante, and L. J. Ignarro, *Effects of nitric oxide on cell proliferation,* (Journal of the American College of Cardiology, 2013) pp. 89–95.

[48] J. B. Swaney, *Mechanisms of protein-lipid interaction. association of apolipoproteins ai and a-ii with binary phospholipid mixtures.* (ASBMB, 1980) pp. 8791–8797.

[49] R. Pertwee, *Cannabinoids,* (Springer Berlin Heidelberg, 2006) Chap. Effect on Cell Viability, pp. 628–638.

[50] A. Parrish, *Nanoprecipitation: Mit microfluidic mixer can synthesize 100 types of nanoparticles per minute for drug delivery,* (2012), ineffableisland consulted on 22-05-2017.

[51] J. Tang, S. Baxter, A. Menon, A. Alaarg, B. L. Sanchez-Gaytan, F. Fay, Y. Zhao, M. Ouimet, M. S. Braza, V. A. Longo, *et al.*, *Immune cell screening of a nanoparticle library improves atherosclerosis therapy,* (National Acad Sciences, 2016) p. 201609629.

[52] M. Durán-Lobato, L. Martín-Banderas, R. Lopes, L. Gonçalves, M. Fernández-Arévalo, and A. Almeida, *Lipid nanoparticles as an emerging platform for cannabinoid delivery: physicochemical optimization and biocompatibility,* (Taylor & Francis, 2016) pp. 190–198.

[53] L. Yetukuri, S. Söderlund, A. Koivuniemi, T. Seppänen-Laakso, P. S. Niemelä, M. Hyvönen, M.-R. Taskinen, I. Vattulainen, M. Jauhiainen, and M. Orešič, *Composition and lipid spatial distribution of hdl particles in subjects with low and high hdl-cholesterol,* (ASBMB, 2010) pp. 2341–2351.

[54] K. J. Hallock, D.-K. Lee, J. Omnaas, H. I. Mosberg, and A. Ramamoorthy, *Membrane composition determines pardaxin's mechanism of lipid bilayer disruption,* (Elsevier, 2002) pp. 1004–1013.

[55] N. Kucerka, D. Marquardt, T. A. Harroun, M.-P. Nieh, S. R. Wassall, D. H. de Jong, L. V. Schäfer, S. J. Marrink, and J. Katsaras, *Cholesterol in bilayers with pufa chains: doping with dmpc or popc results in sterol reorientation and membrane-domain formation,* (ACS Publications, 2010) pp. 7485–7493.

[56] J. Gubernator, *Active methods of drug loading into liposomes: recent strategies for stable drug entrapment and increased in vivo activity,* (Taylor & Francis, 2011) pp. 565–580.

[57] V. Chiurchiù, M. Lanuti, G. Catanzaro, F. Fezza, C. Rapino, and M. Maccarrone, *Detailed characterization of the endocannabinoid system in human macrophages and foam cells, and antiinflammatory role of type-2 cannabinoid receptor,* (Elsevier, 2014) pp. 55–63.

[58] C. L. Westhorpe, E. M. Dufour, A. Maisa, A. Jaworowski, S. M. Crowe, and W. A. Muller, *Endothelial cell activation promotes foam cell formation by monocytes following transendothelial migration in an in vitro model,* (Elsevier, 2012) pp. 220–226.

[59] N. N., *Jwh 133 description,* (2017), cayman chemicals, Michigan consulted on 05-06-2017.

[60] E. L. Tóth, E. G. Holczer, K. Iván, and P. Fürjes, *Optimized simulation and validation of particle advection in asymmetric staggered herringbone type micromixers,* (Multidisciplinary Digital Publishing Institute, 2014) pp. 136–150.

[61] M. S. Williams, K. J. Longmuir, and P. Yager, *A practical guide to the staggered herringbone mixer,* (Royal Society of Chemistry, 2008) pp. 1121–1129.

[62] C. Gärtner, *Lab-on-a-chip catalogue,* (2012), microfluid ChipShop consulted on 09-08-2017.